Molecular Diversity
https://doi.org/10.1007/s11030-023-10650-6

ORIGINAL ARTICLE

Discovery of novel direct small-molecule inhibitors targeting HIF-2α using structure-based virtual screening, molecular dynamics simulation, and MM-GBSA calculations

Behnaz Yazdani[1] · Hajar Sirous[2] · Francisco J. Enguita[3] · Simone Brogi[2,4] · Peter A. C. Wing[5] · Afshin Fassihi[2,6]

Received: 12 November 2022 / Accepted: 11 April 2023

Abstract

Hypoxia-inducible factors (HIFs) are the main regulatory factors implicated in the adaptation of cancer cells to hypoxic stress, which has provoked much interest as an attractive target for the design of promising chemotherapeutic agents. Since indirect HIF inhibitors (HIFIs) lead to the occurrence of various side effects, the need of the hour is to develop direct HIFIs, physically interacting with important functional domains within the HIF protein structure. Accordingly, in the present study, it was attempted to develop an exhaustive structure-based virtual screening (VS) process coupled with molecular docking, molecular dynamic (MD) simulation, and MM-GBSA calculations for the identification of novel direct inhibitors against the HIF-2α subunit. For this purpose, a focused library of over 200,000 compounds from the NCI database was used for VS against the PAS-B domain of the target protein, HIF-2α. This domain was suggested to be a possible ligand-binding site, which is characterized by a large internal hydrophobic cavity, unique to the HIF-2α subunit. The top-ranked compounds, **NSC106416**, **NSC217021**, **NSC217026**, **NSC215639**, and **NSC277811** with the best docking scores were taken up for the subsequent in silico ADME properties and PAINS filtration. The selected drug-like hits were employed for carrying out MD simulation which was followed by MM-GBSA calculations to retrieve the candidates showing the highest in silico binding affinity towards the PAS-B domain of HIF-2α. The analysis of results indicated that all molecules, except the **NSC277811**, fulfilled necessary drug-likeness properties. Four selected drug-like candidates, **NSC106416**, **NSC217021**, **NSC217026**, and **NSC215639** were found to expose the stability profiles within the cavity located inside the PAS-B domain of HIF-2α over simulation time. Finally, the results of the MM-GBSA rescoring method were indicative of the highest binding affinity of **NSC217026** for the binding site of the HIF-2α PAS-B domain among selected final hits. Consequently, the hit **NSC217026** could serve as a promising scaffold for further optimization toward the design of direct HIF-2α inhibitors for cancer therapy.

Keywords Cancer · Hypoxia-inducible factor · Drug discovery · Molecular dynamics simulation · MM-GBSA energy calculation

✉ Hajar Sirous
h_sirous@pharm.mui.ac.ir

✉ Simone Brogi
simone.brogi@unipi.it

[1] Department of Tissue Engineering, Najafabad Branch, Islamic Azad University, Najafabad, Iran

[2] Bioinformatics Research Center, School of Pharmacy and Pharmaceutical Sciences, Isfahan University of Medical Sciences, Isfahan 81746-73461, Iran

[3] Faculdade de Medicina, Instituto de Medicina Molecular João Lobo Antunes, Universidade de Lisboa, Lisbon, Portugal

[4] Department of Pharmacy, University of Pisa, Via Bonanno 6, 56126 Pisa, Italy

[5] Nuffield Department of Medicine, University of Oxford, Oxford, UK

[6] Department of Medicinal Chemistry, School of Pharmacy and Pharmaceutical Sciences, Isfahan University of Medical Sciences, Isfahan 81746-73461, Iran

Published online: 29 April 2023

Introduction

Cancer cells behave differentially when exposed to very low oxygen levels for varying periods. When cancer cells adapt themselves to a hypoxic environment, significant changes in their biological processes are observed. The most prominent metabolic switch toward glycolysis can significantly lead to a decreased pH in the tumor microenvironment [1]. In addition, a hypoxic cancer cell is more resistant to chemotherapy because of the increased expression ratio of drug-resistance genes during hypoxic stress [2]. Cancer cells can relieve the tension of hypoxic stress by expressing angiogenic factors, such as vascular endothelial growth factor protein (VEGF), which induces fibroblast and endothelial cells to form new microvessels to perfuse the tumor microenvironment [3].

Hypoxic pressure can significantly enhance cancer cells' potential for metastasis and migration toward the other host tissues via altering and reforming their extracellular matrix [4]. The major regulatory factors responsible for orchestrating adaptive responses of cancer cells to hypoxic conditions are hypoxia-inducible factors (HIFs). Over the last decade, newer studies have noticed the importance of HIF factors in the regulation of the metabolic pathways, survival and metastatic potential of a variety of hypoxic cancer cells, which lacked enough oxygen supply at the tissue level. Over-expression of the HIF pathway in the tumor microenvironment appears to be one of the common features in almost all solid tumors. Therefore, HIFs have been exploited as one of the valuable molecular targets for the design of promising chemotherapeutic agents [5]. These factors remained popular among researchers through the recent decades of experiments on hypoxic cancers [6, 7].

HIF transcriptional factors are heterodimers composed of alpha (HIF-α) and constitutive ARNT beta (also known as HIF-β) subunits which belong to a large family of basic helix–loop–helix/Per-ARNT-SIM (bHLH–PAS) proteins [8, 9]. Under well-oxygenated conditions, HIF-α subunits are hydroxylated by prolyl hydroxylase (PHD) enzymes and are subjected to rapid proteasomal degradation, leading to HIF suppression.

Yet when oxygen is limited, the activity of the PHD enzymes is inhibited resulting in the stabilization of the HIF-α subunits. The accumulated HIF-α heterodimerizes with HIF-1β and translocates into the nucleus, where HIF-α binds to a hypoxia-response element (HRE), in the promoter regions of the target genes. Ultimately, this binding is followed by the activation of expression of a variety of genes, many of which are coordinately involved in angiogenesis, glycolysis, growth factor signaling, tumor invasion, and metastasis [10]. The protein level of HIF-α subunits depends on the duration and tension of hypoxic stress. Each subunit holds a specific time responsibility to regulate the cell's survival, metabolism, and other critical biological processes that are vital for the adaptation of cancer cells to hypoxia [11, 12]. HIF-1α subunit has been extensively studied and analyzed in hypoxic cancers compared to the isoforms from HIF-α subunits, including HIF-2 α and HIF-3 α [13, 14]. There are many potential molecular mechanisms to inhibit the activity of HIF-α subunits from the initial steps of their cellular translation level to the regulation of protein stability, dimerization, and transcriptional activity. HIF-α subunits can be inhibited either directly via targeting key functional domains in their protein structure, or indirectly through regulation of other molecules in the HIF signaling pathway that eventually affect the stability and activity of the HIF-α as a transcription factor [15].

Indirect inhibitors of HIF-α subunits target upstream signaling proteins such as AKT (Protein kinase B), mammalian target of rapamycin (mTOR), histone deacetylase (HDAC), P300/CBP (CREB-binding protein), and/or the downstream pathways such as anti-VEGF-therapy [16, 17]. Despite those indirect inhibitors have successfully decreased HIF-α protein levels in cellular experiments, most of these inhibitors suffer from high cytotoxicity and various unwanted side effects, limiting their clinical utility [18]. Therefore, the need of the hour significantly is to develop direct and specific inhibitors against HIF-α subunits that physically interact with important functional domains within the HIF-α protein structure [19–21].

In this respect, one of the two PAS domains in HIF-2α (PAS-B) has particularly provided the potential opportunity for the rational design of small-molecule inhibitors. Groundbreaking research demonstrated that the PAS-B domain of HIF-2α possesses a large internal cavity that carries a hydrophobic core unique to the HIF-2α subunit. This well-suited cavity could accommodate ligand binding to induce conformational changes that allosterically attenuate the protein–protein interaction between HIF-2α and ARNT subunits, leading to disruption of HIF heterodimer formation and transcriptional activity (Fig. 1) [22–26].

The discovery of a series of small molecules capable of binding to the PAS-B internal cavity of HIF-2α and so crippling the heterodimerization of the HIF-2α/HIF-β complex validated the HIF-2α as a therapeutic target. In this vein, structure-based design approaches led to disclose some indanol-based derivatives (is also known as PT derivatives) (Fig. 2) with excellent potency as representative inhibitors of HIF-2α [27–29]. In particular, these efforts culminated in the identification of the first HIF-2α antagonist, **PT2385**, to enter to clinical development [30]. Although **PT2385** demonstrated a declined HIF-2-α dependent transcription and tumor growth in heavily pretreated advanced clear cell renal cell carcinoma (ccRCC) patients, it was disadvantaged by

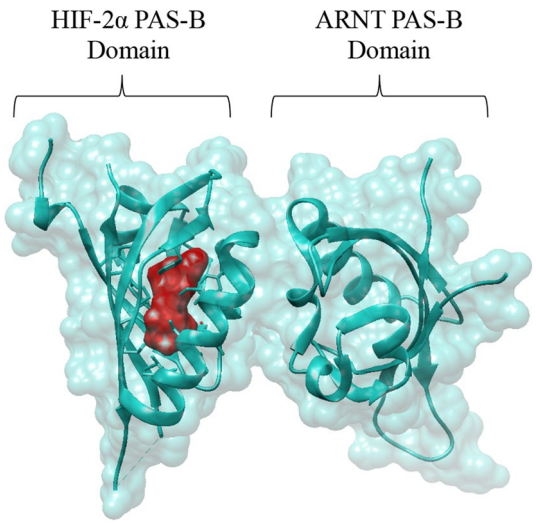

Fig. 1 Representation of the PAS-B heterodimer of HIF-2α with ARNT subunit. The space-filled model of the ligand-binding pocket within the PAS-B domain of HIF-2α is marked in red color

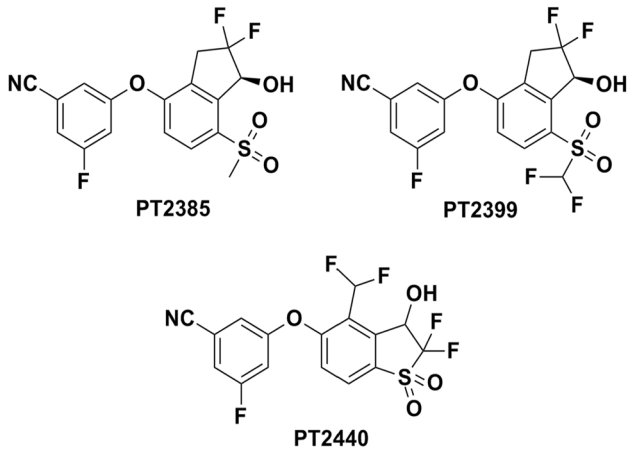

Fig. 2 2D chemical structures of some the representative PT derivatives based on indanol scaffold as HIF-2α inhibitors. These derivatives have been reported by recent studies to directly target and inhibit the PAS-B domain of the HIF-2α subunit and so, prevent its heterodimerization with other subunits, including the ARNT PAS-B domain

highly variable and dose-limited pharmacokinetics related to its extensive metabolism to a glucuronide metabolite by UGT2B17 in the intestine [31]. Thus, this necessitates the demand for continued research to explore new generation of HIF-2 α inhibitors possessing more favorable pharmacokinetic profiles while retaining inhibitory potency [31, 32].

In pursuit of this objective, in the current study, we implemented a reliable structure-based virtual screening (VS) process with the combination of in silico methods (molecular docking, molecular dynamic (MD) simulation, and MM-GBSA calculations) to seek novel direct HIF-2α inhibitors, potentially acting as disruptors of HIF-2α/HIF-β dimerization. For this purpose, a focused library of over 200,000 compounds retrieved from the NCI database was exploited for VS against the PAS-B domain of the target protein, HIF-2α. X-ray structures of the PAS-B domain of the HIF-2α subunit complexed with some small-molecule inhibitors are available in Protein Data Bank. Herein, the recently solved the co-crystal structure of HIF-2α with **PT-2440** (PDB ID: 6D09) has been exploited to efficiently identify hits possessing the potential to bind the PAS-B domain of HIF-2α. Moreover, in silico drug-likeness and physicochemical filters have also been incorporated into this screening to enrich the final hit compounds with desirable drug-like features. The flowchart of the VS process applied in this study is depicted in Fig. 3. The findings obtained here could be served as a foundation for future experimental explorations to motivate the innovative design of a new generation of direct HIF-2α inhibitors.

Materials and methods

Selection of ligand library and datasets

The anti-cancer ligand collection of the National Cancer Institute (NCI) was used in the current study for VS of the molecules, which could act as potential HIF-2α inhibitors. This resulted in a library composed of over 200,000 compounds that have been evaluated by the Developmental Therapeutic Program (DTP) (https://dtp.cancer.gov). DTP is a part of the NCI research platform that specifically focuses on the assessment and development of new chemotherapeutic compounds. DTP has created an 'open' anti-cancer library of compounds, which are a mixture of synthetic and natural molecules. The anti-cancer potential of these molecules was evaluated through two phases of cell-line experiments, including a 3-cell-line screening and a 60-cell-line screening of human cancer cells with multiple doses of treatments. Therefore, the NCI anti-cancer collection was selected for further evaluation by in-silico techniques against the HIF-2α subunit, to filter potential direct molecules that can get further tested in cell-line experiments. The structures of all mined molecules were saved in Structure-Data File (SDF) format and subjected to the next screening steps.

Preparation and optimization of ligand's 3D structures

For a reliable structure-based screening, the structures obtained from the interested library of compounds have to be structurally optimized from a 2D conformation to a 3D energy-minimized conformation. In these conditions, properly optimized ligands can better pursue their optimal pose of binding with the active site of the targeted protein.

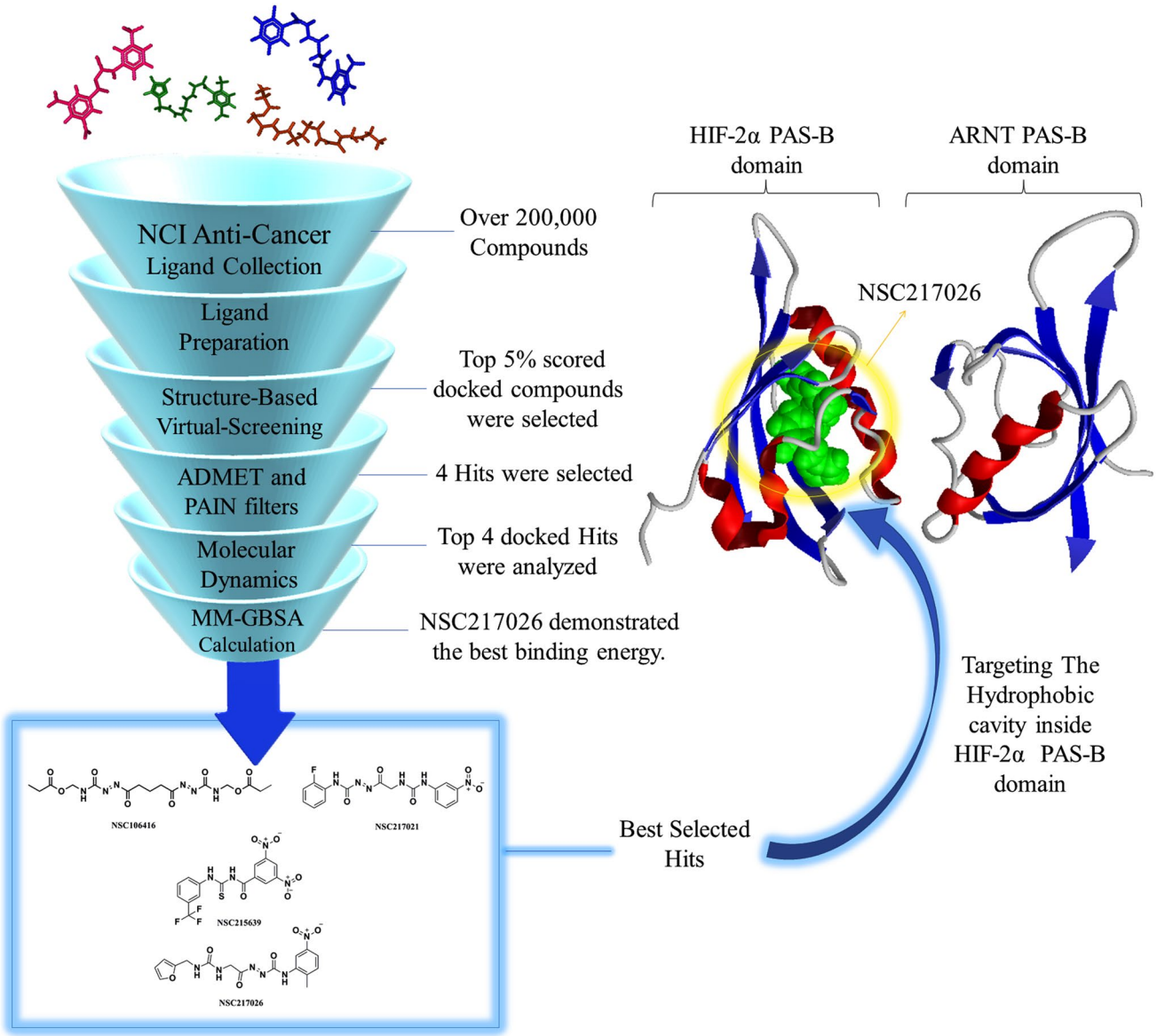

Fig. 3 Flowchart representation of the steps followed for the VS and employed in this study. A large library of compounds with over 200,000 synthetic and natural compounds with anti-cancer potential has been filtered and screened through multiple steps as shown in the flowchart to reach the best potent direct inhibitors against the PAS-B domain of the HIF-2α factor

For this purpose, all the members of the obtained library were treated by the LigPrep module of Schrödinger suite 2015 [33], as previously described by us [34, 35]. This application tool was able to generate the most probable ionization state of the compound's structure at the cellular pH value (7.4 ± 0.5) using the Epik tool [36, 37]. Moreover, molecular energy minimization of the structures was performed using the OPLS-AA_2005 as a force field, which produces the lowest energy conformer for each input ligand [38].

Preparation and optimization of protein's 3D structure

Crystal structure of HIF-2α protein from homosapiens specie (PDB ID: 6D09) was retrieved from the protein data bank (https://www.rcsb.org) [39] to be further prepared using the Protein Preparation Wizard (PPW) module of Schrödinger Suite 2015 [40]. This protocol allowed us to obtain a reasonable starting structure of the target protein for structure-based screening experiments using a series of computational steps [41]. An important step in the preparation of protein

structure is the removal of unnecessary water molecules and ions that are not involved in the binding of the ligand with the protein's active site. The next steps are the addition of missing hydrogen atoms to the initial crystal structure of the protein using the riding model, fixing broken sidechains or missing loops, creating disulfide bonds, and correcting the order of bonds as well. Along these modifications, to optimize the hydrogen bond network, the protonation states of His, Asp, and Glu residues were predicted, 180° rotations of the terminal angle of Asn, Gln, and His residues were assigned, and hydroxyl and thiol hydrogens were sampled. The final step of the preparation is energy minimization with suitable force fields, which results in better protein conformation for further in-silico analyses. Therefore, the OPLS-2005 force filed with a root-mean-square deviation (RMSD) cutoff value of 0.30 Å, was chosen for the energy minimization step that can significantly enhance the stability of protein's structure and its quality for molecular docking and dynamic experiments [38].

Receptor grid generation

Selection of a specific grid box is a necessary step before starting a molecular docking screening process. A grid box is a tridimensional space covering a specific region of interest protein, such as its active site or ligand-binding sites. A grid box is an abstract definition of a certain volume in space within which the search algorithm explores various conformations of the ligands while docking. A good grid box must be large enough to encompass the surrounding surface of the active site and be capable to accommodate the ligands with respect to their size. Considering the goal of the current study for screening direct HIF-2α inhibitors, the grid box was set on a previously reported large water-filled cavity (290 Å) inside the PAS-B domain of HIF-2α, which is surrounded between a beta-sheet and an alpha helix. These studies have indicated that this cavity could be a potential cofactor or ligand-binding site, which could induce conformational alternations, leading to averting HIF-2α heterodimerization with its partner, HIF-β subunit or Aryl Hydrocarbon Receptor Nuclear Translocator (ARNT) [24, 25, 37]. The grid box for the prepared protein was generated using Molegro Virtual Docker software (MVD) [42] and centered on the water-filled cavity inside the PAS-B domain of HIF-2α with the following coordination: $x = 23.06$ Å, $y = -1.18$ Å, $z = -10.97$ Å.

Structure-based virtual screening

The VS module implemented in the Molegro Virtual Docker Software (MVD) [42] was used to identify the top 5% potential ligands with the best MolDock and ReRank scores, among NCI anti-cancer library. The MolDock [Grid] scoring function is a grid-based version of the THOMSEN 2006 scoring function, which orders the top-ranked compounds based on their best pose of binding with the protein's active site and is faster in pre-calculation of potential energy values based on the selected grid box. The ReRank scoring function calculates the binding affinity of ligands to produce a docking score, which is based on the sum of ligand–protein interaction energy and internal energy of the ligand [42]. For docking analysis, the number of runs was set to 50 times, which determines the number of times docking simulations get repeated for each ligand within the library. Further options, such as the optimization of H-bond positions, which can enhance the optimal direction of rotatable H-bonds within the ligand and protein's structure, and Energy minimization were selected to be performed after docking analysis. Finally, the 5 top-ranked ligands, displaying the best MolDock score values lower than − 135.0 kcal/mol, were retrieved for further evaluation by a dynamic simulation technique.

Prediction of ADME properties

SwissADME online web server (www.swissadme.ch) was employed as an extra filter to exclude less pharmacokinetically suitable hits selected from VSW. This step was performed to select only hits that were to be predicted to possess satisfactory physicochemical properties in the appropriate range recommended by the server. Analysis of Lipinski's rule of five and some principal molecular descriptors affecting pharmacokinetic properties were among the important criteria investigated for filtering. Especially, Lipinski's RO5 evaluates the drug-likeness behavior of studied hits which is necessary for rational drug design.

Molecular dynamics simulation

The top 4 ranked candidates based on molecular docking results were subjected to the MD simulation experiments for further evaluating the ligand-binding conformation, stability of their binding mode within the PAS-B domain of HIF-2α and clarification of the ligand–protein interactions in detail. The MD simulation was performed using Desmond 5.6 academic version, provided by D. E. Shaw Research ("DESRES"), employing Maestro as graphical interface [43]. MD was performed using the Compute Unified Device Architecture (CUDA) API on two NVIDIA GPUs. As a first step, the complex derived from docking studies was imported in Maestro and by Desmond system builder was solvated into a cubic box filled with water, simulated by TIP3P model [44]. OPLS force field was used for MD calculations. OPLS-aa (all atom) includes every atom explicitly with specific functional groups and types of molecules including several bio-macromolecules [45, 46]. Na^+ and Cl^- ions were added to provide

a final salt concentration of 0.15 M to simulate physiological concentration of monovalent ions. Constant temperature (300 K) and pressure (1.01325 bar) were employed with NPT (constant number of particles, pressure and temperature) as ensemble class. RESPA integrator was used in order to integrate the equations of motion, with an inner time step of 2.0 fs for bonded and non-bonded interactions within the short-range cutoff [47]. Nose–Hoover thermostats were used to keep the constant simulation temperature [48], and the Martyna–Tobias–Klein method was applied to control the pressure [49]. Long range electrostatic interactions were calculated by particle-mesh Ewald method (PME) [50]. The cutoff for van der Waals and short-range electrostatic interactions was set at 9.0 Å. The equilibration of the system was performed with the default protocol provided in Desmond, which consists of a series of restrained minimizations and MD simulations applied to slowly relax the system. Consequently, one individual trajectory for each complex of 100 ns was calculated. MD simulations experiments were performed also considering a reference inhibitor (**PT-2440**) to obtain a direct comparison. The trajectory files were analyzed by Simulation Event implemented in the Desmond package. The same application was used to generate all plots concerning MD simulation presented in this study. Accordingly, the RMSD was calculated using the following equation:

$$\mathrm{RMSD}_x = \sqrt{\frac{1}{N}\sum_{i=1}^{N}\left(r_i'(t_x) - r_i(t_{\mathrm{ref}})\right)^2},$$

where the RMSD_x is referred to the calculation for a frame x, N is the number of atoms in the atom selection; t_{ref} is the reference time (typically the first frame is used as the reference and it is regarded as time $t = 0$); and r' is the position of the selected atoms in frame x, after superimposing on the reference frame, where frame x is recorded at time t_x. The procedure is repeated for every frame in the simulation trajectory. Regarding the RMSF the following equation was used for the calculation:

$$\mathrm{RMSF}_i = \sqrt{\frac{1}{T}\sum_{t=1}^{T}\left\langle\left(r_i'(t) - r_i(t_{\mathrm{ref}})\right)^2\right\rangle},$$

where RMSF_i is referred to a generic residue i, T is the trajectory time over which the RMSF is calculated, t_{ref} is the reference time, r_i is the position of residue i; r' is the position of atoms in residue i after superposition on the reference, and the angle brackets indicate that the average of the square distance is taken over the selection of atoms in the residue.

Ligand-binding free energy estimation based on MM-GBSA technique

The free energy calculation analysis provides a worthwhile predictive criterion to rank compounds with respect to their binding affinities [51, 52]. Thus, the MD trajectories of the HIF-2α protein in complex with the selected inhibitors from previous MD simulations were analyzed using the MM-GBSA technique. The evaluation of the ligand free energy for each ligand (ΔG_{bind} in kcal/mol) was performed using the MM-GBSA technique implemented in Maestro environment. The consequent ligand-binding free energy (ΔG_{bind}) was estimated using the following equation: $\Delta G_{\mathrm{bind}} = \Delta E_{\mathrm{MM}} + \Delta G_{\mathrm{solv}} + \Delta G_{\mathrm{SA}}$; where ΔE_{MM} represents the difference in the minimized energies calculated for the ligand–receptor complex and the sum of the energies of the unbounded receptor and ligands. ΔG_{solv} denotes the difference in the Generalized Born Surface Area (GBSA) solvation energy of the ligand–receptor complex and the sum of the unbounded receptor and ligands. ΔG_{SA} represents the difference in the surface area energies for the ligand–receptor complex and the sum of the surface area energies for the unbounded receptor and ligands [53, 54]. The thermal MM-GBSA script available in Desmond (*thermal_mmgbsa.py*) [55] was used to evaluate the ΔG_{bind} for the selected complexes. This tool used the Desmond MD trajectory, splitting it into individual frame snapshots, and runs each one through MM-GBSA analysis. During the MM-GBSA calculation, 1000 snapshots from the 100 ns MD simulation were used as input to compute the average binding free energy. The evaluated ΔG_{bind} are reported as average values in the "Results and discussion" section along with the energy components used in the calculation.

Results and discussion

Virtual screening and hit identification

VS studies of the commercial database are a fruitful resource for the identification of potentially bioactive molecules for a given drug target. The primary advantage of such methods is the significant decrease in overall time, costs, and resources associated with the development of a newfangled drug and pre-clinical research. In this regard, structure-based VS is quantitatively capable of predicting the accurate binding mode of ligands within the active site of the target protein, thereby preferentially ranking them in decreasing order of their binding affinities [56]. Thus, the starting NSC anticancer library (almost 300,000 compounds) was screened against the HIF-2α subunit, targeting the PAS-B domain, using the VS procedure available in the Molegro Virtual Docker environment. Accurate binding affinity prediction between protein and ligand through molecular docking requires careful optimization of their 3D structures. Therefore, the X-ray structure of the HIF-2α protein was optimized in the protein preparation wizard, applying the OPLS-2005 force field to remove bad atomic contacts in the 3D

structure and to obtain a structure with a lower energy state. Furthermore, the ligand preparation at the cellular pH value (7.4 ± 0.5) using LigPrep and taking into account possible ionization states guaranteed that all ligands are in the lowest energy conformation.

The grid box was placed on the previously reported water-filled cavity inside the PAS-B domain of HIF-2α (PDB ID: 6D09) and VS mode was set to retrieve the hit compounds with the best binding affinity towards the ligand-binding site. This method greatly reduced the number of initial compounds to 5% of the starting library, thereby enriching the library with more promising virtual hits. To validate the applied docking protocol, the co-crystallized inhibitor **PT-2440** was re-docked within the PAS-B domain of the protein and its binding mode was explored. The analysis of the re-docking results divulged a similar binding mode of **PT-2440** to that seen in its parent crystal structure in complex with HIF-2α. The root-mean-square deviation (RMSD) value for the predicted conformation of this compound in comparison with its coordination in the crystal structure was 0.14. Superimposition of the two structures of **PT 2440**, the best re-docked pose and the ligand in the co-crystal structure are provided in Fig. 4. As shown in this figure, the re-docked **PT-2440** occupied a relatively hydrophobic region within PAS-B domain of HIF-2α that is surrounded by the amino acid residues Phe_{280}, Tyr_{307}, Arg_{308}, Leu_{319}, Phe_{244}, Ser_{246}, Leu_{296}, Val_{302}, Gly_{323}, Ser_{304}, Ser_{292}, Met_{289}, Thr_{321} and Ile_{261}. As a result, these residues were found to be involved in the favorable hydrophobic interactions with **PT-2440**. As can be seen in the Table 1, these interactions were augmented by hydrogen binding formation with crucial residues His_{293}, Ser_{304}, Ser_{292} and Asn_{341}. Moreover, several kinds of Pi interactions were observed with residues Phe_{254}, Tyr_{281}, His_{248}, Ala_{277}, Met_{252}, Ile_{337}, Met_{309} and Cys_{339} that contribute to further stability of ligand in the binding site.

Satisfied with the validity of the docking procedure, the members of virtual library were docked into the same binding site of the HIF-2α. After screening, the compounds were sorted by MolDock and Re-rank scores, and final hit selection was conducted based on obtaining the minimum MolDock score. consequently, this filter rendered five top-ranked hits, **NSC106416**, **NSC217021**, **NSC21706**, **NSC215639**, and **NSC277811** as potential inhibitors to continue the further examination. The chemical structures of these compounds are shown in Fig. 5. All information of five selected compounds including docking score values and key residues involved in the intermolecular interactions are summarized in Table 1. Visual scrutiny also revealed that the best binding pose of the five selected molecules engaged the same internal cavity in the PAS-B domain of HIF-2α as **PT-2440**, providing appropriate hydrophobic and hydrogen bond interactions. A close-up view of the best-docked pose of the five top-ranked hits interacting with key amino acids inside the hydrophobic cavity of the HIF-2α PAS-B domain along with their 2D interaction diagram is depicted in Fig. 6.

As shown in Fig. 6, the predicted binding mode of these hits was predominantly driven by the extensive hydrophobic interactions by amino acid residues such as Ile_{337}, Val_{302},

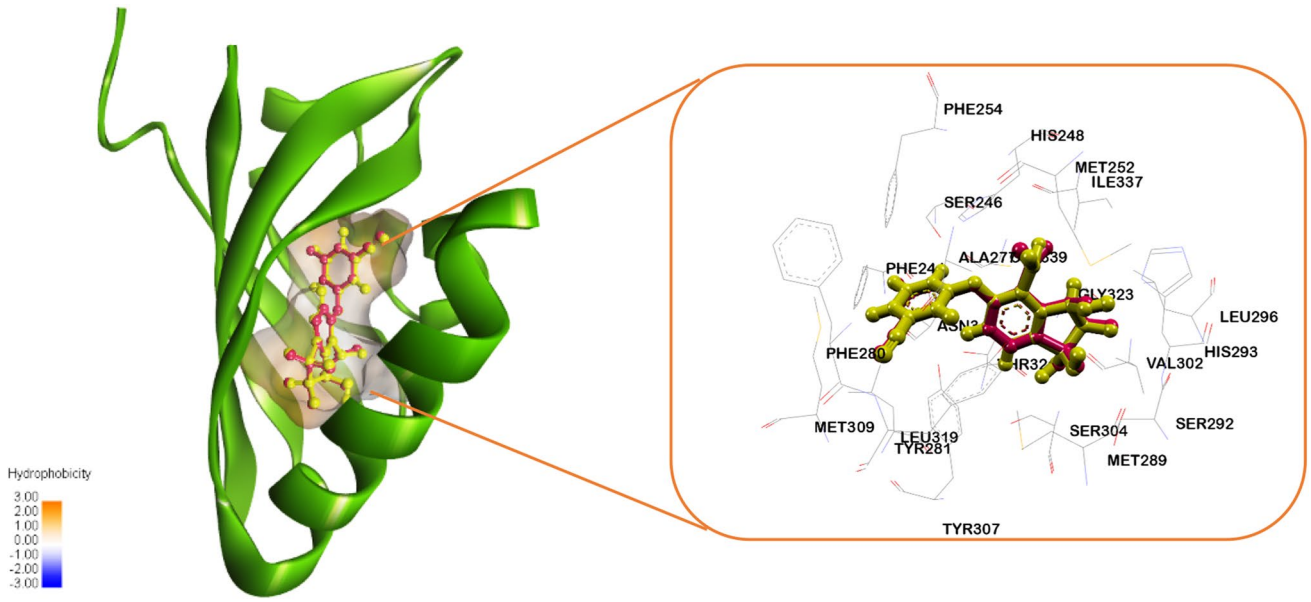

Fig. 4 Comparison of the two bound conformations of the reference ligand, **PT-2440**, inside the PAS-B cavity of HIF-2α along with a detailed zoom into the prominent interacting amino acids of binding site: the pink model shows the X-ray crystallographic orientation, and the best re-docked pose is shown as a yellow model. The solid ribbon model displays the backbone of PAS-B domain of HIF-2α, while key interacting residues are shown as stick models

Table 1 Interaction details for five top-ranked compounds resulting from docking into the hydrophobic cavity of HIF-2α PAS-B domain using structure-based VS

Entry	Mol Dock score	Re-rank score	Amino acids involved in interactions		
			Hydrophobic interactions	Hydrogen bond interactions	Pi interactions
NSC106416	− 170.10	− 103.49	Phe_{280}, Ala_{277}, Phe_{254}, Ile_{261}, Phe_{244}, Ala_{277}, Leu_{319}, Val_{302}, Thr_{321}, Thr_{324}, Met_{252}, Ser_{304}, Ser_{292}, Met_{289}	Tyr_{307}, Ser_{246}, Asn_{341}, 3*His_{293}, Gly_{323}, Cys_{339}	Leu_{292}, Thr_{281}, Ile_{337}, Met_{309} (pi-Alkyl)
NSC217021	− 158.13	− 105.00	Gly_{323}, Thr_{321}, Phe_{244}, Phe_{254}, Ala_{277}, Phe_{280}, Tyr_{281}, Ser_{292}, His_{248}, Tyr_{307}, Leu_{296}, Leu_{319}, Ile_{337}, Val_{302}, Val_{303}	Cys_{339}, Asn_{341}, Ser_{246}, Ser_{304}, Gly_{323}	Met_{252} (Pi-Sulfur); Met_{309}, Ala_{277}, Met_{289} (Pi-Alkyl)
NSC215639	− 135.27	− 92.27	Ser_{292}, Gly_{323}, Leu_{296}, Ser_{304}, Met_{252}, Ile_{337}, Ile_{261}, Phe_{244}, His_{248}, Leu_{319}, Phe_{280}, Tyr_{307}	Tyr_{281}, Asn_{341}, 2*Ser_{246}, $Ser_{304,}$ Gly_{323}	His_{293}, Met_{309}, Cys_{339} (Pi-Sulfur); Phe_{254} (Pi–Pi); Ala_{277}, Met_{289} (Pi-Alkyl)
NSC217026	− 176.05	− 128.53	Thr_{290}, Val_{302}, Leu_{296}, Thr_{321}, Ile_{337}, Phe_{254}, Phe_{280}, Ala_{277}, Leu_{319}, Gly_{323}, Ile_{265}, Ile_{261}, Phe_{244}, His_{248}	Ser_{304}, Cys_{339}, Ser_{246}, Asn_{341}, 2*Tyr_{307}, Gly_{323}, Ala_{277}	Met_{252} (Pi-Sulfur), Met_{289}, Tyr_{281}, Met_{309} (Pi-Alkyl)
NSC277811	− 174.92	− 139.8	Ser_{292}, His_{248}, Tyr_{281}, Met_{309}, Ala_{277}, Thr_{321}, His_{293}, Tyr_{307}	Tyr_{281}, His_{293}, Tyr_{307}, Ala_{277}, Met_{309}, Thr_{321}	Val_{302}, Met_{289}, Ile_{337}, Met_{252} (Pi-Alkyl) Cys_{339} (Pi-Sulfur)
PT-2440	− 151.04	− 119.84	Phe_{280}, Tyr_{307}, Arg_{308}, Leu_{319}, Phe_{244}, Ser_{246}, Leu_{296}, Val_{302}, Gly_{323}, Ser_{304}, Ser_{292}, Met_{289}, Thr_{321}, Ile_{261}	His_{293}, Ser_{304}, Ser_{292}, Asn_{341}	Phe_{254}, Tyr_{281}, His_{248} (Pi–Pi stacking) Ala_{277}, Met_{252}, Ile_{337} (Pi-Alkyl) Met_{309}, Cys_{339} (Pi-Sulfur)

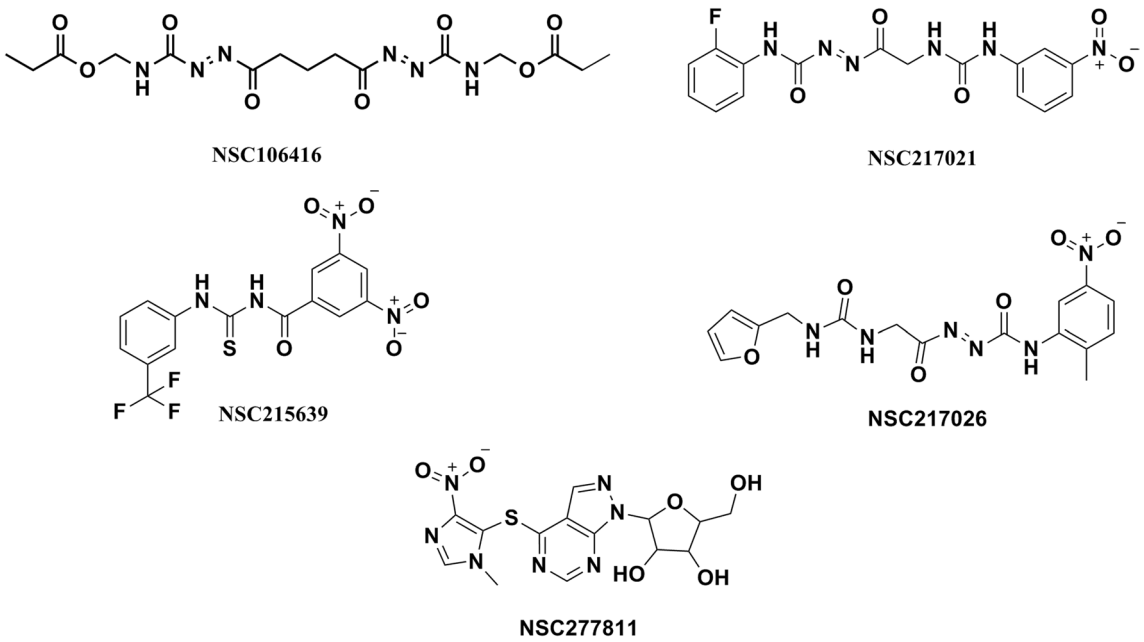

Fig. 5 2D Chemical structures of the top 5 hits with the best predicted binding affinities found by structure-based VS studies within NCI anti-cancer library as possible HIF-2α inhibitor

Leu_{319}, Leu_{296}, Phe_{244}, and Phe_{280}. Moreover, the obtained results pointed out that Ser_{246}, Asn_{341}, Tyr_{307}, Cys_{339}, and His_{293} were substantial amino acid residues in the holding of molecules in the binding site through multiple hydrogen bond interactions. Further stability of the ligands in the binding cavity was owed to the various parallel pi interactions

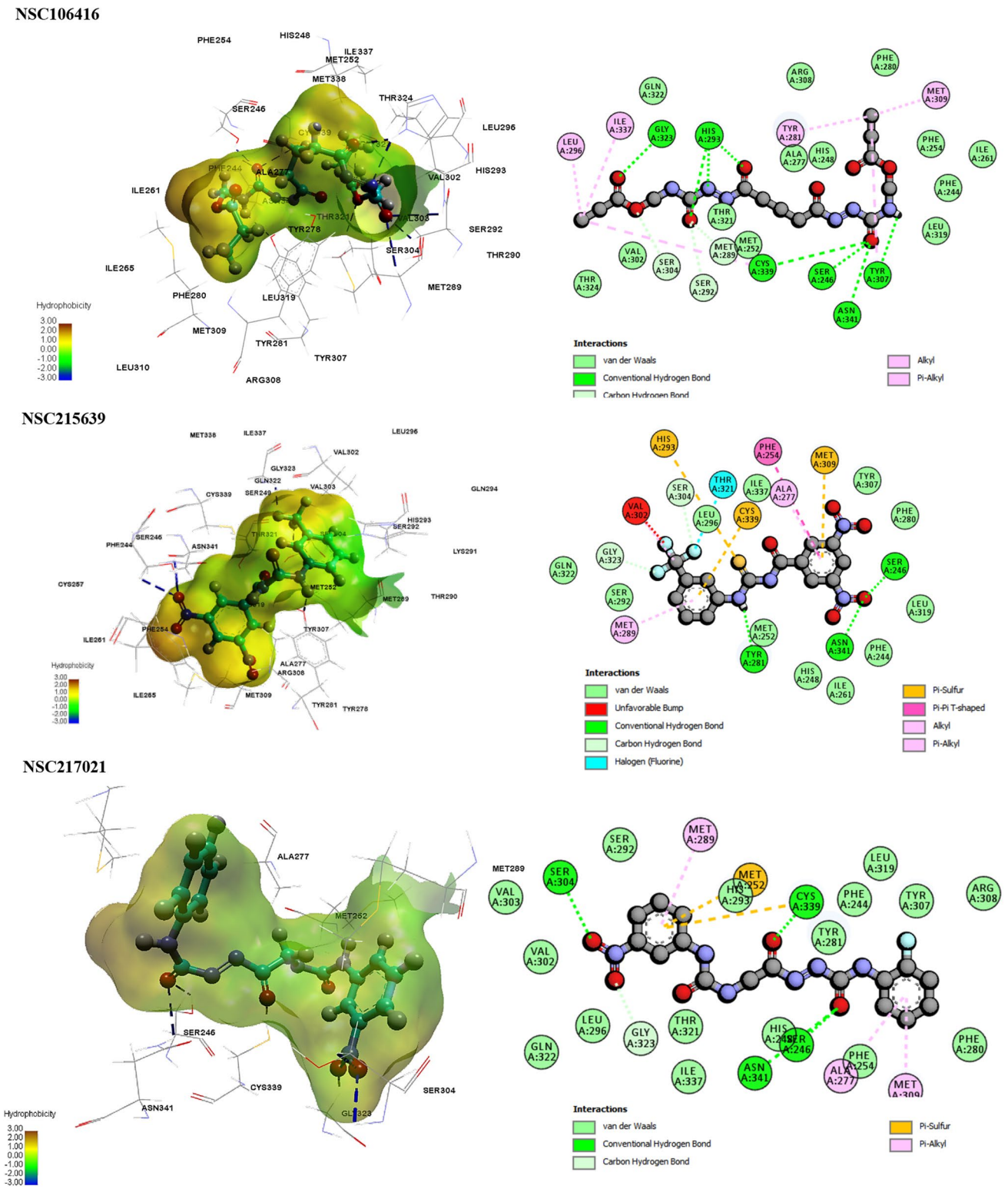

Fig. 6 (**Left**) 3D representation of the putative-binding mode of the five top-scored hits as well as known inhibitor, **PT-2440**, inside the hydrophobic cavity of HIF-2α PAS-B domain. In each case, the ligand in the binding site is shown as ball and stick model, and colored by elements, while the key interacting amino acid residues of binding site are represented by stick models. Hydrogen bonds are marked as blue dash lines. (**Right**) The representation of the 2D interaction diagram of the five top-screened ligands and **PT-2440** with the important amino acid residues inside the hydrophobic cavity of the HIF-2α PAS-B domain. The figures were created using the Accelrys discovery studio visualizer software

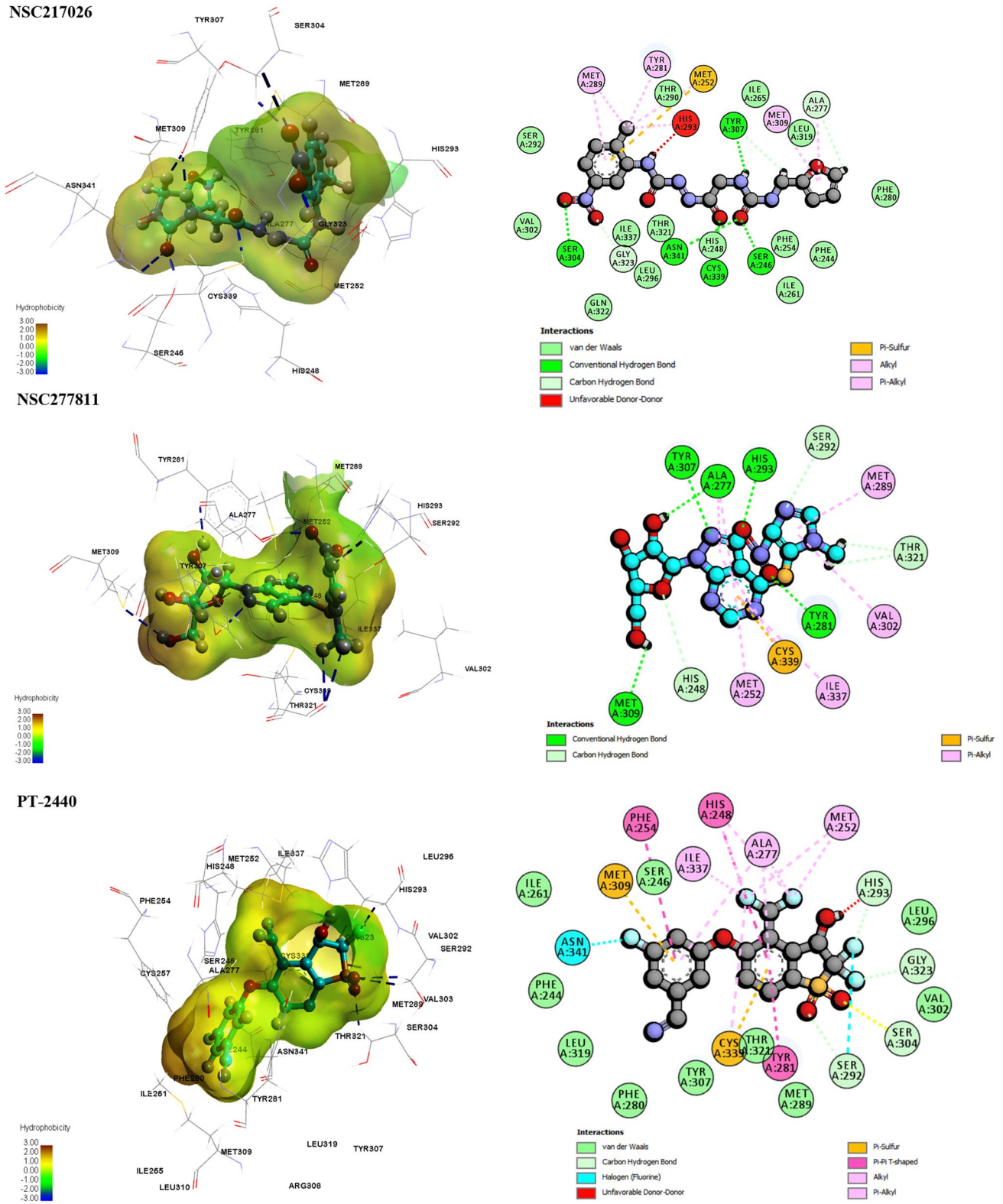

Fig. 6 (continued)

(pi–pi, pi-sulfur, and pi-alky types) which were responsible for fruitful contacts between the ligand and some of the crucial amino acid residues such as Phe_{254}, Met_{309}, Met_{289}, and Cys_{339} (see Table 1). Based on the results seen in Table 1, among 5 potential hits, molecules **NSC106416**, **NSC217021**, **NSC217026**, and **NSC277811**, specially **NSC217026** (MolDock score − 176.05 kcal/mol), were predicted to have more negative MolDock score values (ranged from − 176.05 to − 158.13 kcal/mol) than reference compound, **PT-2440** (− 151.04 kcal/mol). The cavity inside HIF-2α PAS-B domain has been known to have a hydrophobic profile. Therefore, the difference in the binding scores, could be due to greater range of amino acids that were predicted to participates in hydrophobic and Pi Interactions. This implies that these compounds with higher in silico binding a*ffi*nities, probably stand as the most stable ligands in the HIF-2α PAS-B internal cavity. Among these compounds, compound **NSC217026** with the lowest MolDock score particularly exhibited the highest number of molecular interactions via hydrogen bonds and various pi contacts.

Analysis of Lipinski and physiochemical properties

In the early stages of rational drug design campaigns, the elimination of the weak druggable candidates and focus on the compounds with more likely successful drug-like properties is of utmost importance. The inclusion of a pharmacokinetics profile in the drug candidate selection can improve the probability of clinical success, thereby speeding up lead identification. Nowadays, in silico techniques are widely used for the fast prediction of pharmacokinetic properties, known as ADMET, of new chemical entities preceding expensive experimental procedures [57, 58]. Thus as a part of the current study, the SwissADME free web server was applied for in silico assessment of drug-like behavior of five hit molecules selected from the VSW through the prediction of some key physicochemical parameters and "Lipinski's rule of five" (RO5). Lipinski's RO5 is widely used as the criterion for a description of four important physicochemical properties via defining ranges derived from FDA-approved drugs, which are known to have clinically acceptable ADME properties in the human body. This rule states that a favorable drug-like molecule should have: (1) a partition coefficient (log*P*) ≤ 5; (2) a molecular weight (MW) ≤ 500 g mol^{-1}; (3) several hydrogen bond acceptors ≤ 10 (notably N and O atoms); (4) a number of hydrogen bond donors ≤ 5 (OH and NH groups). Any value differing from these values was considered a violation. The acceptable value of RO5 violations for a drug-like molecule is 1 [59]. As seen in Table 2, among five selected hits, three molecules lacked any Lipinski violations and thereby signified to possess appropriate drug-like potential. The results also indicate that all molecules, except the **NSC277811**, concurred with the acceptable range defined for the partition coefficient between octanol and water (log*P*). Compound **NSC277811** exhibited a value of log*P* slightly out of the allowed limit. This physicochemical property, in turn, fits with Lipinski's RO5 and remarkably affects the distribution, oral absorption, and permeability properties of compounds within the body through the biological membranes. In addition, this molecule was found to have PSA (202.46 Å), polar surface area, more than the maximum permissible limit (200.0 Å). This descriptor holds a great influence on drug bioavailability and shown to correlate well with passive molecular transport across the membranes [60]. QPlogKhsa is another

Table 2 The ADMET prediction of four top hits obtained from structure-based VS

Entry	H-bond donor ≤ 5	H-bond acceptor ≤ 10	Molecular weight (g/mol) ≤ 500	log*P*[a] ≤ 5	PSA[b] (Å^2)	QPlogKhsa[c]	Rule of five[d]	PAINS alert[e]
NSC106416	6	8	418.40	1.66	193.06	− 0.306	1	0
NSC217021	5	6	390.33	0.83	157.18	− 0.233	0	0
NSC215639	1	8	414.32	1.55	164.86	0.666	0	0
NSC217026	5	6	390.35	1.38	170.32	− 0.273	0	0
NSC277811	3	10	409.38	− 2.14	202.46	− 0.83	1	0
PT-2440	1	10	405.296	1.899	90.962	− 0.323	0	0

The selected physicochemical properties were calculated using SwissADME online web server (www.swissadme.ch)

[a]log*P* predicted octanol/water partition coefficient (acceptable range or recommended value for 95% of known drugs -2-6.5)

[b]PSA predicted Van der Waals surface area of polar nitrogen and oxygen atoms and carbonyl carbon atoms (acceptable range or recommended value for 95% of known drugs 7-200.0)

[c]QPlogKhsa predicted binding to human serum albumin (acceptable range or recommended value for 95% of known drugs -1.5-1.5)

[d]Predicted number of violations of Lipinski's rule of five. The rules are: MW < 500, *P*log*P* < 5, donorHB ≤ 5, accptHB ≤ 10 (acceptable range or recommended value is maximum 1)

[e]Predicted capability to behave as false positives or pan assay interference compounds (PAINS) in VS (recommended value is 0)

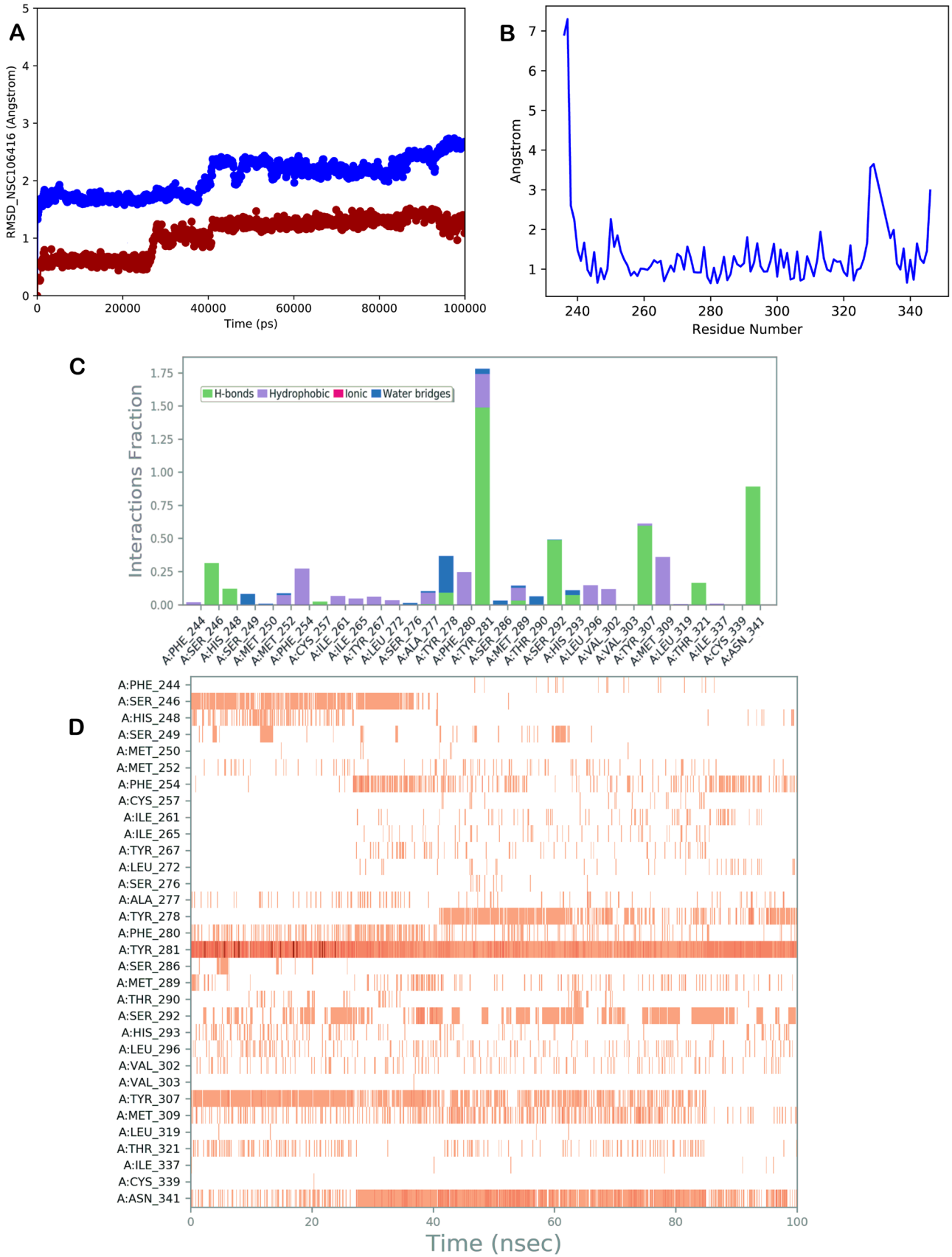

◂**Fig. 7** **A** RMSD calculation for the complex PAS-B domain of HIF-2α**/NSC106416** investigated in this study: protein (blue line) and ligand (red line); **B** RMSF calculation of the PAS-B domain of HIF-2α; **C**, **D NSC106416** monitored in the course of the MD run. The interactions can be grouped into four types: H-bonds (green), hydrophobic (gray), ionic (magenta), and water bridges (blue). The subsequent diagram of the figure illustrates a timeline description of the main interactions. A darker hue of orange indicates that some residues make many distinct contacts with the ligand (Maestro, Schrödinger LLC, release 2020-3)

crucial property reflecting the binding degree of the drug molecule to the proteins within blood plasma such as human serum albumin. It is noteworthy that the binding of drugs to plasma proteins reduces the quantity of the free drug in blood circulation. The predicted values revealed that all of the selected hits are compliant with the prescribed range of this parameter. Thus, selected molecules are likely to circulate freely within the bloodstream, possessing accessibility to the target site. Further, hits were inspected for their potential capability to behave as pan assay interference compounds (PAINS). The PAINS compounds tend to nonspecifically react with a wide range of biological targets instead of specifically affecting one desired target, providing false positive compounds [61]. Based on this criterion, all hits have no sub-structural features that marked them as "frequent hitters" in high-throughput screenings. Overall, results suggest that 4 out of 5 molecules (in Table 2) satisfy both Lipinski's RO5 and desired pharmacokinetic properties. Consequently, to limit the number of drug-like virtual hits, these molecules were selected as final survivors from this step to proceed to the further in silico experiments.

Molecular dynamic (MD) simulation analysis

MD simulation is one of the fundamental in silico techniques for gaining insights into ligand-induced conformational changes and fluctuations in the protein structure on the time scales through introducing atomic-level perturbations. Unlike molecular docking, in MD simulations, the nature of macromolecules is allowed to be highly flexible and dynamic and more similar to their biologically relevant systems in cellular physiological conditions [62]. Thus, using the best binary complexes of the four final selected hits with the PAS-B domain of HIF-2α as the starting point, a 100 ns MD simulation was performed in an explicit hydration environment. The main objective of MD simulations was to ensure the stability of the proposed binding mode of ligands within the target binding site of HIF-2α as a function of simulation time. To assess the binding immovability, structural properties, and convergence of the system during the simulation time, the resulting MD trajectories for all complexes were analyzed through different standard simulation parameters. In this regard, overall structural fluctuations and conformational stability of each complex were evaluated by analyzing the Root-mean-square deviation (RMSD) of the protein backbone and alpha carbon atoms versus simulation time. The RMSD demonstrates the deviation of atoms in the protein's structure during the MD simulation time. The RMSD value of alpha carbons in the protein's structure should be smaller than 2 Å during the phase that the system has been equilibrated. The higher the RMSD value is, the more conformational changes the system has experienced. The flatter RMSD slope that appeared during the time of simulation is a good indicator of a more stable system. In contrast, a high range of fluctuations seen in the RMSD graph implies an unstable binding of the ligand to the desired protein structure.

In general and considering the all the selected complexes, the RMSD plots of selected hits showed that the mentioned complexes reached an equilibrium status and then remained stable throughout the simulation after few nanoseconds. Moreover, the variation of RMSD values is limited, suggesting that all compounds folded into a more stable state than the starting structure during the time of the simulation. Accordingly, the observed binding stability of the analyzed systems well bolstered the credibility of previous docking outcomes, indicating a stabilized binding mode of these compounds with target cavity inside the PAS-B domain of HIF-2α under the given simulation conditions. A comparison between the RMSD plots revealed that **NSC217026** had the least fluctuations in RMSD, thus the most stability during the MD simulations compared to three other hits under the same MD simulation conditions. This compound had a rising in the first 20 ns and then rapidly reached an overall stability, whereas the bound state of other compounds revealed a longer equilibration time.

Root-mean-square fluctuation (RMSF) measurement is a useful method to provide an overall perspective of the dynamic behavior of individual residues in the protein backbone based on their location and involvement in the interaction with a specific ligand. This analysis provides a better perspective to identify the flexible regions in the protein structure. The higher value of RMSF indicates the higher amount of atomic fluctuation of the atomic Cα coordinates of the protein from its average position within the MD simulations. As shown in RMSD plots, the overall pattern of residue fluctuations in studied complexes was found to be almost similar to that of HIF-2α protein in complex with **PT-2440**. The all selected complexes showed a limited fluctuation with the exclusion of a restricted number of residues at the N- and C-terminal ends that are far from the ligand-binding site. In this regard, the key residues interacting with ligand in the

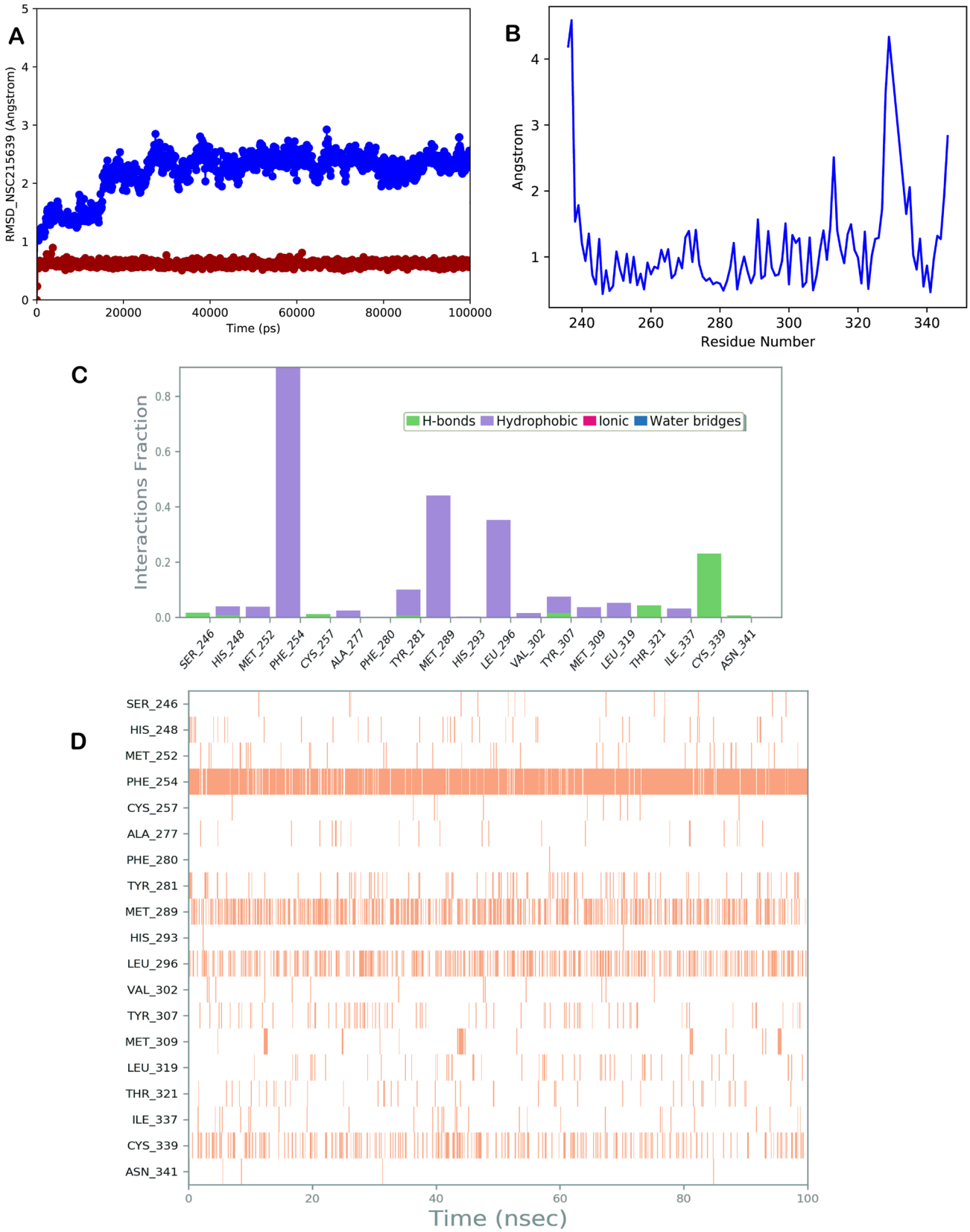

◂**Fig. 8** **A** RMSD calculation for the complex PAS-B domain of HIF-2α/**NSC215639** investigated in this study: protein (blue line) and ligand (red line); **B** RMSF calculation of the PAS-B domain of HIF-2α; **C**, **D** **NSC215639** monitored in the course of the MD run. The interactions can be grouped into four types: H-bonds (green), hydrophobic (gray), ionic (magenta), and water bridges (blue). The subsequent diagram of the figure illustrates a timeline description of the main interactions. A darker hue of orange indicates that some residues make many distinct contacts with the ligand (Maestro, Schrödinger LLC, release 2020-3)

HIF-2α binding site such as Phe_{244}, Tyr_{281}, His_{293}, Met_{309}, Cys_{339} and Asn_{341} exposed rigid behavior with the lowest amounts of fluctuations (RMSF < 1 Å) in the all MD simulation experiments. The low flexibility of these residues verified their capability for formation of stable interaction with ligand compared to other residues in HIF-2α binding site.

This small range of RMSFs demonstrated that ligands were capable to form stable and suitable interactions with the protein-binding site during MD simulation. These results were in perfect accordance with the findings from the analysis of the RMSD plot.

The MD trajectories of each ligand were also analyzed to gain more comprehensive information about intermolecular interactions using the tools available in Desmond software reporting a timeline evaluation of the binding of ligands. Starting from compound **NSC106416**, we described the most relevant interactions found during over the course of simulation. The output of this analysis is reported in Fig. 7. As observed in plots Fig. 7C and D, the compound was able to maintain the binding mode found by molecular docking studies, establishing strong polar interactions with the following residues Tyr_{281}, Ser_{292}, Tyr_{307}, and Asn_{341} through several H-bond interaction. In particular, the stable hydrogen bond formed by Tyr_{281} residue was almost permanently preserved in the whole simulation. While additional polar contacts were also detected with the Phe_{244} and Thr_{321}, hydrophobic interactions could be established with Phe_{254}, Phe_{280}, Tyr_{281}, and Met_{309} that fortified the stability of the retrieved binding mode.

The output of the MD analysis for compound **NSC215639** is reported in Fig. 8. As indicated in plots Fig. 8C and D, the binding mode of this compound was primarily mediated by a strong network of hydrophobic interactions. In this regard, the key lipophilic residues Phe_{254}, Tyr_{281}, Met_{289}, Leu_{296}, and Tyr_{307} were particularly targeted for establishment of various hydrophobic contacts with ligand during the simulation. In particular, this ligand was able to maintain hydrophobic interaction with Phe_{254} during entire simulation time. In addition to the contacts found by docking studies, the formation of a favorable H-bond with the residue Cys_{339} also contributes to the significant binding affinity of this compound within the selected binding site.

The MD analysis of **NSC217021** is illustrated in Fig. 9. As shown in plots Fig. 9C and D, the main contacts found by docking studies of this compound were reproduced during MD simulation. Furthermore, The 100 ns MD simulation was deciphered the formation of additional strong contacts with the residues His_{248}, Tyr_{281}, and His_{293} as well as Leu_{296} through H-bond and hydrophobic interactions, respectively.

As reported in Fig. 10, the pattern of interaction observed in docking model of hit compound **NSC217026** was preserved during MD simulation. The MD analysis well confirmed that residues Tyr_{281}, Ser_{246}, His_{248}, and Asn_{341} were the main hydrogen-bond-interacting residues with this ligand. In particular, Tyr_{281} was found as interacting residue that regularly participated in H-bond formation throughout the simulation time. In line with the docking studies, this residue appears to be one of the crucial residues within the ligand-binding pocket of HIF-2α. Moreover, this compound was sporadically involved in additional contacts with Tyr_{267}, Leu_{272}, Met_{289} (hydrophobic interactions), and Ser_{292} (H-bond), leading to further improving the binding affinity of this compound for the selected binding site.

Finally, the MD results obtained for the co-crystallized ligand (**PT-2440**) were analyzed, comparing the stability and the established contacts within the HIF-2α-binding pocket with respect to the output gained for the compounds selected by VS. As indicated in Fig. 11, the stability of protein–ligand complex was found to be almost similar to the previous analyses with small fluctuations of the system. The ligand **PT-2440** strongly maintained the most favorable contacts found by molecular docking with small variations, such as the interactions with Phe_{254}, Ser_{292}, and His_{293}. In addition, residues Tyr_{281} and Met_{289} were detected to be appropriate for making new strong contacts in the form of hydrophobic and water mediated H-bonds with the **PT-2440**.

Considering insignificant variations of interactions with the crucial residues in the binding site during MD of the selected compounds, it is plausible to believe that identified molecules are capable of tightly binding to the PAS-B domain of HIF-2α with the reasonable thermodynamic stability. To further corroborate this hypothesis, we also conducted a ligand-binding energy calculation applied on the MD simulation trajectories for each presented complex. The output is reported in the next section.

Binding-free energy analysis based on MM-GBSA calculations

The accurate prediction of the binding affinity of top-ranked hits in VS protocols is an important task to prioritize the screened compounds with high confidence for chemical synthesis and biological evaluations. The scoring functions used by various docking tools ignore the flexibility of the protein target and some essential thermodynamic factors in

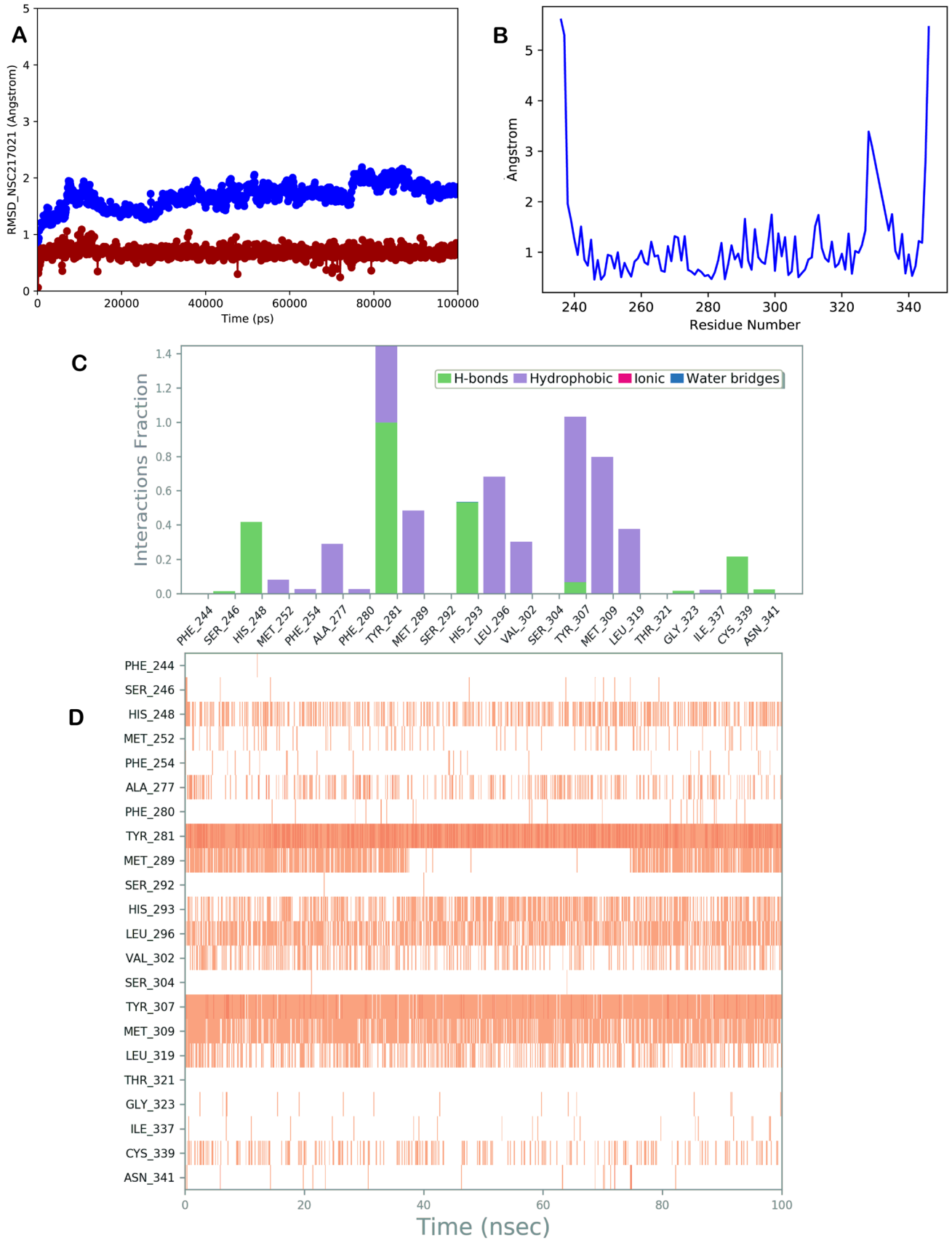

◂**Fig. 9** **A** RMSD calculation for the complex PAS-B domain of HIF-2α/**NSC217021** investigated in this study: protein (blue line) and ligand (red line); **B** RMSF calculation of the PAS-B domain of HIF-2α; **C**, **D** **NSC217021** monitored in the course of the MD run. The interactions can be grouped into four types: H-bonds (green), hydrophobic (gray), ionic (magenta), and water bridges (blue). The subsequent diagram of the figure illustrates a timeline description of the main interactions. A darker hue of orange indicates that some residues make many distinct contacts with the ligand (Maestro, Schrödinger LLC, release 2020-3)

the prediction of free binding energy such as protein and ligand solvation energy terms, and as a consequence, their accuracy in ranking compounds based on their binding affinities is quite weak [63, 64]. Recently, updated methods have considered a combination of molecular mechanical force fields with continuum solvation models, such as MM-GBSA enables us to make more accurate predictions of the free binding energy of ligands from MD trajectories. Considering that all calculations in MM-GBSA are based on the initial and final states of MD simulations, this method has recently emerged as one of the "end-point" approaches in drug discovery protocols. This approach can predict the contributions of a range of important interactions including both polar and non-polar types in the protein–ligand-binding event [65, 66]. Thus, in the last step of our computational workflow, the trajectory models obtained from the previous MD simulations were submitted to the MM-GBSA calculation to further substantiate the binding affinity of top-ranked hits with favorable thermodynamics towards the target binding site. The predicted ΔG_{bind} of the final selected hits along with their contributions to the total binding free energy from various energy components are provided in Table 3.

As shown in Table 3, all compounds were predicted to be potent, having negative binding free energy values (ΔG_{bind}), ranging from 86.18 to − 101.72 kcal/mol. These values were found to be more negative with respect to the reference compound **PT-2440**. Accordingly, the MM-GBSA analysis demonstrated that among the 4 candidates, the most favorable binding energy was scored by **NSC217026** with ΔG_{bind} value of − 101.72 kcal/mol. The superior binding energy of **NSC217026** correlated with higher values of van der Waals (− 73.81 kcal/mol) and electrostatic (− 39.06 kcal/mol) interaction energies (Table 3). This indicates that this compound was more stable than others in the protein-binding site, thereby possessing the highest in silico binding affinity towards the PAS-B cavity of HIF-2α. Interestingly, this finding was in accordance with the better MolDock score of this hit (− 176.05 kcal/mol) compared to the other three hits estimated from preliminary VS experiments. The binding energy of **NSC217026** also correlated with its RMSD graph, which indicated a stable binding with the PAS-B domain of the HIF-2α factor during the MD simulation. Among three other hits, **NSC 215639** exhibited relatively close binding energy (− 92.56 kcal/mol) with respect to the best hit, **NSC217026**.

The general inspection of the free energy components in Table 3 revealed that the van der Waals interaction energy (ΔG_{vdW}) is the most important contributor to the ligands binding energy. This observation emphasizes the critical importance of hydrophobic interactions in the stability of the ligand–protein complexes, which is logical considering the highly hydrophobic nature of the hydrophobic cavity inside the PAS-B domain of HIF-2α.

Conclusion

In the present study, owing to the substantial responsibility of HIFs in the adaptation of cancer cells exposed to hypoxic stress, efforts aimed at identifying new small-molecule inhibitors against the HIF-2α subunit. This subunit has been known to have a large and unique internal hydrophobic cavity within its PAS-B domain, which has been considered a compelling therapeutic target in antineoplastic drug design during the past decade. Therefore, we developed a reliable structure-based VS process with the combination of in silico methods to discover potent direct HIF-2α inhibitors from the NCI database using structural information of the HIF-2α PAS-B domain co-crystallized with ligand **PT-2440**. In this respect, computational evaluation of a starting library of over 200,000 compounds was performed in several hierarchical filtering steps to reduce the number of screened compounds to an enriched set of the most promising candidates. The exploited filtering criteria in the order of steps included: (1) the estimated MolDock score values lower than − 135.0 kcal/mol obtained from the structure-based VS; (2) having satisfactory pharmacokinetic and ADME profiles within the acceptable range described for a drug-like molecule as predicted by using SwissADME web server; (3) MD simulation studies to disclose conformational and binding stability of top drug-like virtual hits within the ligand-binding site of HIF-2α; (4) The best binding free energy values calculated using MM-GBSA method.

The structure-based VS resulted in the final selection of five top-ranked hits: **NSC106416**, **NSC217021**, **NSC217026**, **NSC215639**, and **NSC277811** with favorable docking scores. In addition, the detailed binding modes of all five compounds revealed their vital hydrogen bond and hydrophobic interactions with binding pocket's residues of HIF-2α PAS-B domain such as Phe_{254}, Tyr_{281}, His_{293}, Phe_{280}, His_{248}, Cys_{339}, Asn_{341}, and Met_{309}. These molecules, except the **NSC277811**, satisfied the standard drug-likeness properties for human purposes and lacked false positive warnings during PAINS analysis. The analysis of MD simulation trajectories showed a significant stability of four selected drug-like hits bound to the target cavity inside the PAS-B domain

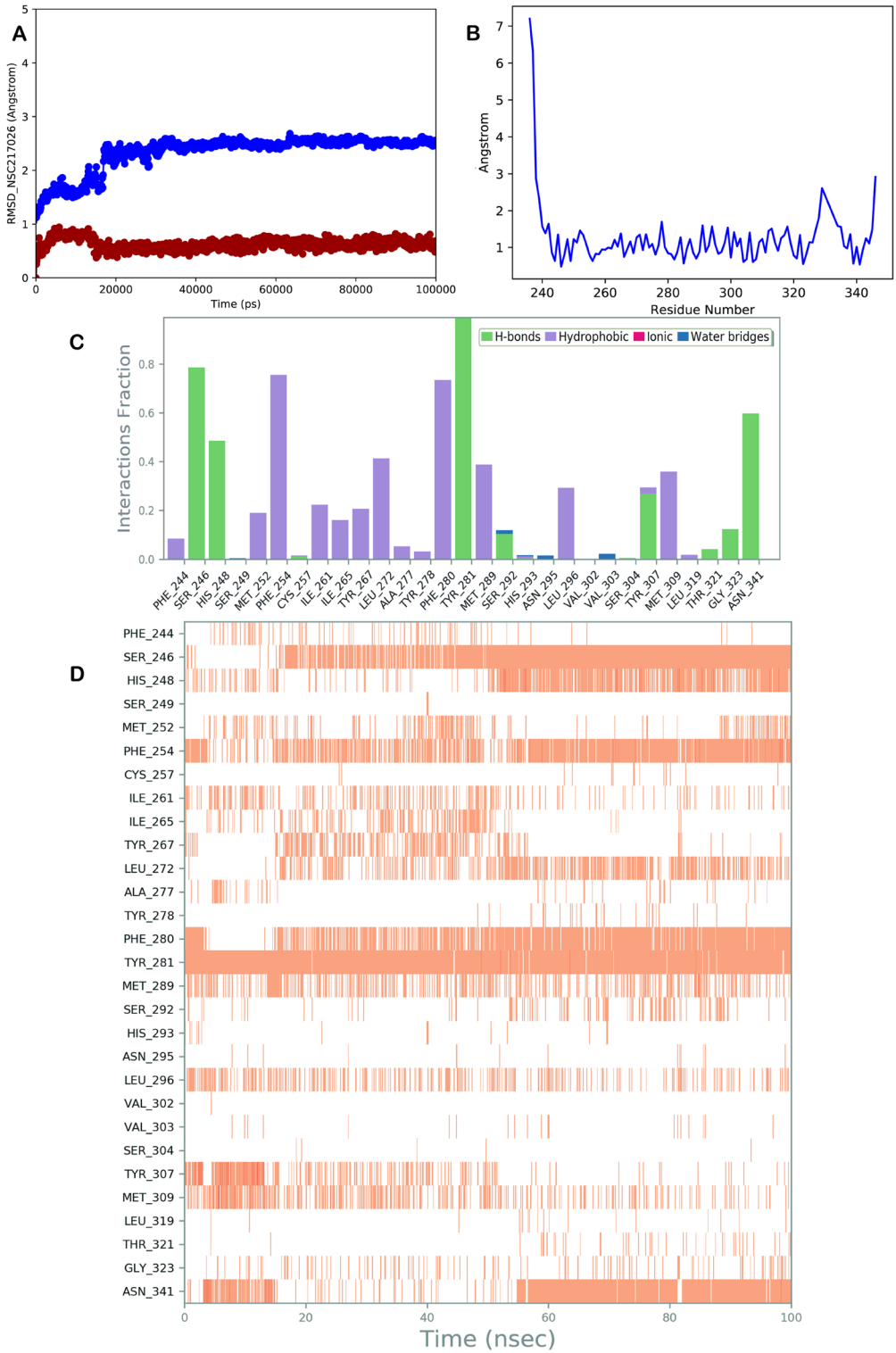

Fig. 10 **A** RMSD calculation for the complex PAS-B domain of HIF-2α/**NSC217026** investigated in this study: protein (blue line) and ligand (red line); **B** RMSF calculation of the PAS-B domain of HIF-2α; **C**, **D** **NSC217026** monitored in the course of the MD run. The interactions can be grouped into four types: H-bonds (green), hydrophobic (gray), ionic (magenta), and water bridges (blue). The subsequent diagram of the figure illustrates a timeline description of the main interactions. A darker hue of orange indicates that some residues make many distinct contacts with the ligand (Maestro, Schrödinger LLC, release 2020-3)

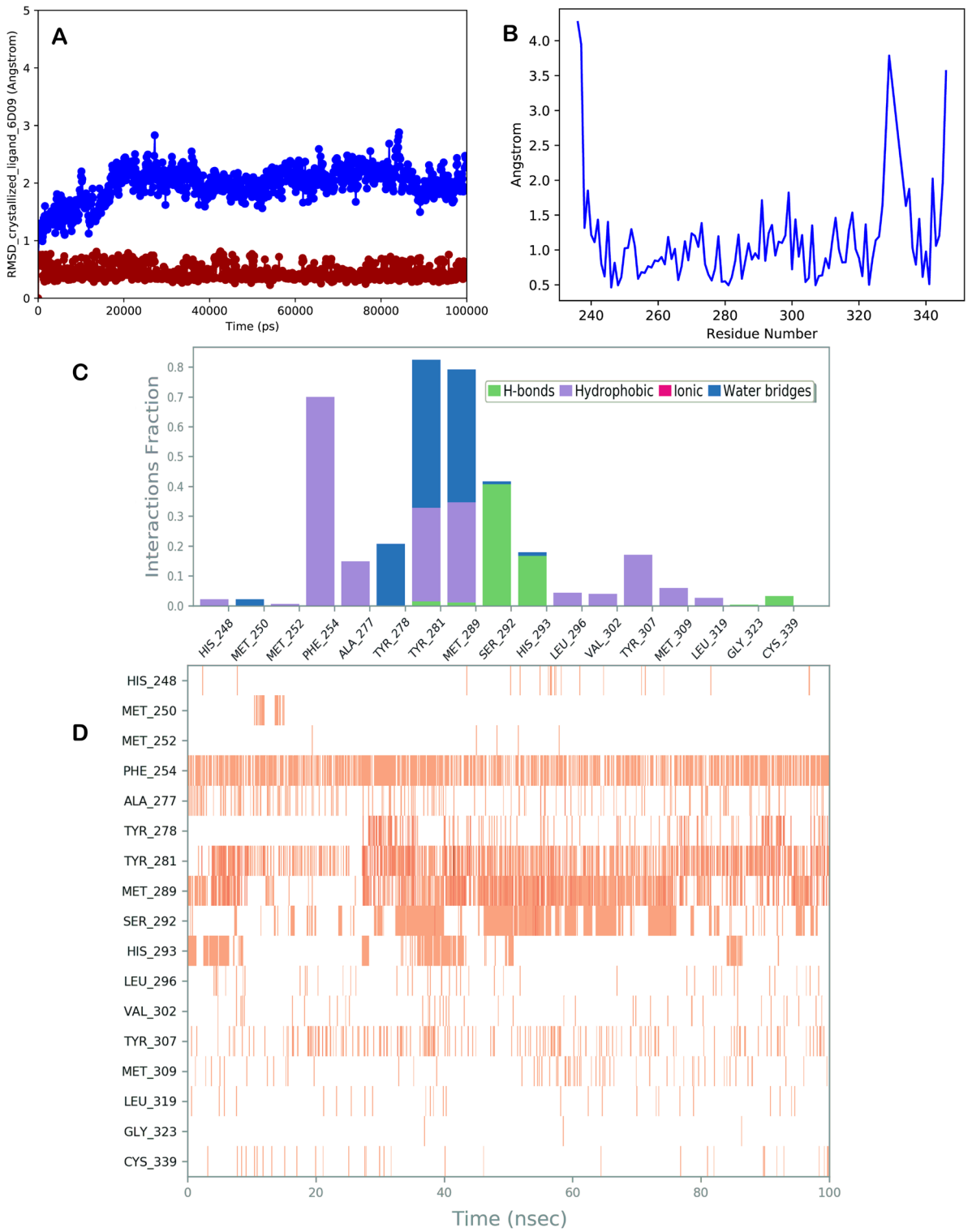

Fig. 11 **A** RMSD calculation for the complex PAS-B domain of HIF-2α/**PT-2440** investigated in this study: protein (blue line) and ligand (red line); **B** RMSF calculation of the PAS-B domain of HIF-2α; **C**, **D PT-2440** monitored in the course of the MD run. The interactions can be grouped into four types: H-bonds (green), hydrophobic (gray), ionic (magenta), and water bridges (blue). The subsequent diagram of the figure illustrates a timeline description of the main interactions. A darker hue of orange indicates that some residues make many distinct contacts with the ligand (Maestro, Schrödinger LLC, release 2020-3)

Table 3 Predicted free binding energies (Δ*G*bind) from the MM-GBSA calculation and the energy components of the best-ranked compounds in comparison with the reference molecule **PT-2440**

Entry	ΔG_{vdw}[a] (kcal/mol)	ΔG_{coul}[b] (kcal/mol)	ΔG_{Hbond}[c] (kcal/mol)	ΔG_{Lipo}[d] (kcal/mol)	ΔG_{Pack}[e] (kcal/mol)	ΔG_{SolGB}[f] (kcal/mol)	ΔG_{bind}[g] (kcal/mol)
NSC217026	− 73.81	− 39.06	− 2.83	− 24.76	− 2.94	31.17	− 101.72
NSC215639	− 72.43	− 19.47	− 1.77	− 25.82	− 3.28	25.04	− 92.56
NSC217021	− 69.36	− 26.52	− 1.86	− 23.93	− 2.07	26.62	− 88.71
NSC106416	− 66.59	− 24.78	− 2.34	− 13.61	0.00	23.82	− 86.18
PT-2440	− 58.21	− 18.24	− 0.79	− 21.15	− 2.89	14.56	− 83.26

[a]Contribution of van der Waals interaction energy to the binding free energy

[b]Contribution of Coulomb energy to the binding free energy

[c]Hydrogen-bonding contribution to the binding free energy

[d]lipophilic energy contribution to the binding free energy

[e]π–π packing energy contribution to the binding free energy

[f]Generalized Born electrostatic solvation energy contribution to the binding free energy

[g]Total binding free energy

of HIF-2α compared to the reference drug, **PT-2440**. At the final point of our screening workflow, the results of the MM-GBSA calculation, in comparison with the reference drug **PT-2440**, were indicative of the best binding energy of **NSC217026** and thereof highest binding affinity towards the binding site of HIF-2α PAS-B domain among the selected final hits. This finding was in satisfactory agreement with the results of molecular docking and MD simulation and so supported the credibility of our VS strategy. Consequently, the hit **NSC217026** could be considered as an encouraging template for the development of the next generation of anti-cancer agents with direct inhibitory potential against the PAS-B domain of **HIF**-2α. In this context, future experimental investigations of this compound on hypoxic cancer cells would be suggested to provide explicit indications for the design of analogous structures with improved pharmacological features and properties.

Acknowledgements The authors would like to thank the Bioinformatics Research Center in Isfahan University of Medical Sciences, Isfahan, I.R. Iran for financing and supporting this project (Grant No. 299006 to H.S).

Author contributions BY and HS designed research. BY, FJE, SB, PACW, and HS compiled and analyzed data. BY, FJE, SB, and HS performed computations. BY, SB, and HS wrote the manuscript. HS supervised the project.

Funding The study was supported by Isfahan University of Medical Sciences (Grant No. 299006).

Data availability Relevant data associated with this study are contained within the article or in supplementary material.

Code availability Not applicable.

Declarations

Conflict of interest The authors declare that they have no conflicts of interest.

Ethical approval This is a purely computational study and ethics approvals are not applicable.

Consent to participate Not applicable.

Consent for publication All co-authors have read and approved the manuscript.

References

1. Vaupel P, Mayer A (2007) Hypoxia in cancer: significance and impact on clinical outcome. Cancer Metastasis Rev 26(2):225–239. https://doi.org/10.1007/s10555-007-9055-1
2. Graham K, Unger E (2018) Overcoming tumor hypoxia as a barrier to radiotherapy, chemotherapy and immunotherapy in cancer treatment. Int J Nanomed 13:6049. https://doi.org/10.2147/ijn.s140462
3. Liao D, Johnson RS (2007) Hypoxia: a key regulator of angiogenesis in cancer. Cancer Metastasis Rev 26(2):281–290. https://doi.org/10.1007/s10555-007-9066-y
4. Lu X, Kang Y (2010) Hypoxia and hypoxia-inducible factors: master regulators of metastasis. Clin Cancer Res 16(24):5928–5935. https://doi.org/10.1158/1078-0432.ccr-10-1360
5. Akanji MA, Rotimi D, Adeyemi OS (2019) Hypoxia-inducible factors as an alternative source of treatment strategy for cancer. Oxid Med Cell Longev 2019:8547846. https://doi.org/10.1155/2019/8547846
6. Wang B, Zhao Q, Zhang Y, Liu Z, Zheng Z, Liu S, Meng L, Xin Y, Jiang X (2021) Targeting hypoxia in the tumor microenvironment: a potential strategy to improve cancer immunotherapy. J Exp Clin Cancer Res 40(1):24. https://doi.org/10.1186/s13046-020-01820-7

7. Jing X, Yang F, Shao C, Wei K, Xie M, Shen H, Shu Y (2019) Role of hypoxia in cancer therapy by regulating the tumor microenvironment. Mol Cancer 18(1):157. https://doi.org/10.1186/s12943-019-1089-9
8. Ke Q, Costa M (2006) Hypoxia-inducible factor-1 (HIF-1). Mol Pharmacol 70(5):1469–1480. https://doi.org/10.1124/mol.106.027029
9. Greer SN, Metcalf JL, Wang Y, Ohh M (2012) The updated biology of hypoxia-inducible factor. EMBO J 31(11):2448–2460. https://doi.org/10.1038/emboj.2012.125
10. Webb JD, Coleman ML, Pugh CW (2009) Hypoxia, hypoxia-inducible factors (HIF), HIF hydroxylases and oxygen sensing. Cell Mol Life Sci 66(22):3539–3554. https://doi.org/10.1007/s00018-009-0147-7
11. Déry M-AC, Michaud MD, Richard DE (2005) Hypoxia-inducible factor 1: regulation by hypoxic and non-hypoxic activators. Int J Biochem Cell Biol 37(3):535–40. https://doi.org/10.1016/j.biocel.2004.08.012
12. Semenza GL (2001) Hypoxia-inducible factor 1: oxygen homeostasis and disease pathophysiology. Trends Mol Med 7(8):345–350. https://doi.org/10.1016/s1471-4914(01)02090-1
13. Patel SA, Simon MC (2008) Biology of hypoxia-inducible factor-2 α in development and disease. Cell Death Differ 15(4):628–634. https://doi.org/10.1038/cdd.2008.17
14. Duan C (2016) Hypoxia-inducible factor 3 biology: complexities and emerging themes. Am J Physiol Cell Physiol 310(4):C260–C269. https://doi.org/10.1152/ajpcell.00315.2015
15. Choudhry H, Harris AL (2018) Advances in hypoxia-inducible factor biology. Cell Metab 27(2):281–298. https://doi.org/10.1016/j.cmet.2017.10.005
16. Burroughs SK, Kaluz S, Wang D, Wang K, Van Meir EG, Wang B (2013) Hypoxia inducible factor pathway inhibitors as anticancer therapeutics. Future Med Chem 5(5):553–572. https://doi.org/10.4155/fmc.13.17
17. Tang W, Zhao G (2020) Small molecules targeting HIF-1α pathway for cancer therapy in recent years. Bioorg Med Chem 28(2):115235. https://doi.org/10.1016/j.bmc.2019.115235
18. Fallah J, Rini BI (2019) HIF inhibitors: status of current clinical development. Curr Oncol Rep 21(1):6. https://doi.org/10.1007/s11912-019-0752-z
19. Hu C-J, Sataur A, Wang L, Chen H, Simon MC (2007) The N-terminal transactivation domain confers target gene specificity of hypoxia-inducible factors HIF-1α and HIF-2α. Mol Biol Cell 18(11):4528–4542. https://doi.org/10.1091/mbc.e06-05-0419
20. Brahimi-Horn MC, Pouysségur J (2009) HIF at a glance. J Cell Sci 122(8):1055–1057. https://doi.org/10.1242/jcs.035022
21. Li Z, You Q, Zhang X (2019) Small-molecule modulators of the hypoxia-inducible factor pathway: development and therapeutic applications. J Med Chem 62(12):5725–5749. https://doi.org/10.1021/acs.jmedchem.8b01596
22. Scheuermann TH, Li Q, Ma HW, Key J, Zhang L, Chen R, Garcia JA, Naidoo J, Longgood J, Frantz DE, Tambar UK, Gardner KH, Bruick RK (2013) Allosteric inhibition of hypoxia inducible factor-2 with small molecules. Nat Chem Biol 9(4):271–276. https://doi.org/10.1038/nchembio.1185
23. Key J, Scheuermann TH, Anderson PC, Daggett V, Gardner KH (2009) Principles of ligand binding within a completely buried cavity in HIF2alpha PAS-B. J Am Chem Soc 131(48):17647–17654. https://doi.org/10.1021/ja9073062
24. Scheuermann TH, Stroud D, Sleet CE, Bayeh L, Shokri C, Wang H, Caldwell CG, Longgood J, MacMillan JB, Bruick RK, Gardner KH, Tambar UK (2015) Isoform-selective and stereoselective inhibition of hypoxia inducible factor-2. J Med Chem 58(15):5930–5941. https://doi.org/10.1021/acs.jmedchem.5b00529
25. Scheuermann TH, Tomchick DR, Machius M, Guo Y, Bruick RK, Gardner KH (2009) Artificial ligand binding within the HIF2α PAS-B domain of the HIF2 transcription factor. Proc Natl Acad Sci USA 106:450–455. https://doi.org/10.1073/pnas.0808092106
26. Erbel PJ, Card PB, Karakuzu O, Bruick RK, Gardner KH (2003) Structural basis for PAS domain heterodimerization in the basic-helix–loop–helix-PAS transcription factor hypoxia-inducible factor. Proc Natl Acad Sci USA 100:15504–15509. https://doi.org/10.1073/pnas.2533374100
27. Wehn PM, Rizzi JP, Dixon DD, Grina JA, Schlachter ST, Wang B, Xu R, Yang H, Du X, Han G, Wang K (2018) Design and activity of specific hypoxia-inducible factor-2α (HIF-2α) inhibitors for the treatment of clear cell renal cell carcinoma: discovery of clinical candidate (S)-3-((2,2-difluoro-1-hydroxy-7-(methylsulfonyl)-2,3-dihydro-1H-inden-4-yl)oxy)-5-fluorobenzonitrile (PT2385). J Med Chem 61(21):9691–9721. https://doi.org/10.1021/acs.jmedchem.8b01196
28. Cho H, Du X, Rizzi JP, Liberzon E, Chakraborty AA, Gao W, Carvo I, Signoretti S, Bruick RK, Josey JA, Wallace EM, Kaelin WG (2016) On-target efficacy of a HIF-2alpha antagonist in preclinical kidney cancer models. Nature 539:107–111. https://doi.org/10.1038/nature19795
29. Wallace EM, Rizzi JP, Han G, Wehn PM, Cao Z, Du X, Cheng T, Czerwinski RM, Dixon DD, Goggin BS, Grina JA, Halfmann MM, Maddie MA, Olive SR, Schlachter ST, Tan H, Wang B, Wang K, Xie S, Xu R, Yang H, Josey JA (2016) A smallmolecule antagonist of HIF2alpha is efficacious in preclinical models of renal cell carcinoma. Cancer Res 76(18):5491–5500. https://doi.org/10.1158/0008-5472.can-16-0473
30. Chen W, Hill H, Christie A, Kim MS, Holloman E, Pavia-Jimenez A, Homayoun F, Ma Y, Patel N, Yell P, Hao G, Yousuf Q, Joyce A, Pedrosa I, Geiger H, Zhang H, Chang J, Gardner KH, Bruick RK, Reeves C, Hwang TH, Courtney K, Frenkel E, Sun X, Zojwalla N, Wong T, Rizzi JP, Wallace EM, Josey JA, Xie Y, Xie X-J, Kapur P, McKay RM, Brugarolas J (2016) Targeting renal cell carcinoma with a HIF-2 antagonist. Nature 539:112–117. https://doi.org/10.1038/nature19796
31. Courtney KD, Infante JR, Lam ET, Figlin RA, Rini BI, Brugarolas J, Zojwalla NJ, Lowe AM, Wang K, Wallace EM, Josey JA, Choueiri TK (2018) Phase I dose escalation trial of PT2385, a first-in-class hypoxia inducible factor-2α antagonist in patients with previously treated advanced clear cell renal cell carcinoma. J Clin Oncol 36:867–874. https://doi.org/10.1200/jco.2017.74.2627
32. Xu R, Wang K, Rizzi JP, Huang H, Grina JA, Schlachter ST, Wang B, When PM, Yang H, Dixon DD, Czerwinski RM (2019) 3-[(1S,2S,3R)-2,3-difluoro-1-hydroxy-7-methylsulfonylindan-4-yl]oxy-5-fluorobenzonitrile (PT2977), a hypoxia-inducible factor 2α (HIF-2α) inhibitor for the treatment of clear cell renal cell carcinoma. J Med Chem 62:6876–6893
33. Schrödinger LLC (2015) Version 3.3, LigPrep. Schrödinger, LLC, New York
34. Sirous H, Chemi G, Gemma S, Butini S, Debyser Z, Christ F, Saghaie L, Brogi S, Fassihi A, Campiani G, Brindisi M (2019) Identification of novel 3-hydroxypyran-4-one derivatives as potent HIV-1 integrase inhibitors using in silico structure-based combinatorial library design approach. Front Chem 7:574. https://doi.org/10.3389/fchem.2019.00574
35. Sirous H, Campiani G, Calderone V, Brogi S (2021) Discovery of novel hit compounds as potential HDAC1 inhibitors: the case of ligand-and structure-based virtual screening. Comput Biol Med 137:104808. https://doi.org/10.1016/j.compbiomed.2021.104808
36. Epik (2015) Epik version 3.4. Schrödinger, LLC, New York
37. Shelley JC, Cholleti A, Frye LL, Greenwood JR, Timlin MR, Uchimaya M (2007) Epik: a software program for pK a prediction and protonation state generation for drug-like molecules. J

Comput Aided Mol Des 21:681–691. https://doi.org/10.1007/s10822-007-9133-z
38. Jorgensen WL, Maxwell DS, Tirado-Rives J (1996) Development and testing of the OPLS all-atom force field on conformational energetics and properties of organic liquids. J Am Chem Soc 118:11225–11236. https://doi.org/10.1021/ja9621760.10.1021/acs.jctc.9b00054
39. Bernstein FC, Koetzle TF, Williams GJ, Meyer JF, Brice MD, Rodgers JR, Kennard O, Shimanouchi T, Tasumi M (1977) The Protein Data Bank: a computer-based archival file for macromolecular structures. J Mol Biol. https://doi.org/10.1016/S0022-2836(77)80200-3
40. Protein preparation wizard 2015, -1; Epik version 2.4, Schrödinger, LLC, New York, 2015; Impact version 5.9, Schrödinger, LLC, New York, 2015; Prime version 3.2, Schrödinger, LLC, New York, 2015
41. Sastry GM, Adzhigirey M, Day T, Annabhimoju R, Sherman W (2013) Protein and ligand preparation: parameters, protocols, and influence on virtual screening enrichments. J Comput Aided Mol Des 27:221–234. https://doi.org/10.1007/s10822-013-9644-8
42. Thomsen R, Christensen MH (2006) MolDock: a new technique for high-accuracy molecular docking. J Med Chem 49(11):3315–3321. https://doi.org/10.1021/jm051197e
43. Desmond Molecular Dynamics System, version 5.6, D. E. Shaw Research, New York, 2018. Maestro-Desmond Interoperability Tools, Schrödinger, New York, 2018
44. Jorgensen WL, Chandrasekhar J, Madura JD, Impey RW, Klein ML (1983) Comparison of simple potential functions for simulating liquid water. J Chem Phys 79:926–935. https://doi.org/10.1063/1.445869
45. Jorgensen WL, Maxwell DS, Tirado-Rives J (1996) Development and testing of the OPLS all-atom force field on conformational energetics and properties of organic liquids. J Am Chem Soc 118:11225–11236. https://doi.org/10.1021/ja9621760
46. Brogi S, Sirous H, Calderone V, Chemi G (2020) Amyloid β fibril disruption by oleuropein aglycone: long-time molecular dynamics simulation to gain insight into the mechanism of action of this polyphenol from extra virgin olive oil. Food Funct 11(9):8122–8132. https://doi.org/10.1039/D0FO01511C
47. Humphreys DD, Friesner RA, Berne BJ (1994) A multiple-time-step molecular dynamics algorithm for macromolecules. J Phys Chem 98:6885–6892. https://doi.org/10.1021/j100078a035
48. Hoover WG (1985) Canonical dynamics: equilibrium phase-space distributions. Phys Rev A 31:1695. https://doi.org/10.1103/PhysRevA.31.1695
49. Martyna GJ, Tobias DJ, Klein ML (1994) Constant pressure molecular dynamics algorithms. J Chem Phys 101:4177–4189. https://doi.org/10.1063/1.467468
50. Essmann U, Perera L, Berkowitz ML, Darden T, Lee H, Pedersen LGA (1995) Smooth particle mesh Ewald method. J Chem Phys 103:8577–8593. https://doi.org/10.1063/1.470117
51. Huang N, Kalyanaraman C, Irwin JJ, Jacobson MP (2006) Physics-based scoring of protein–ligand complexes: enrichment of known inhibitors in large-scale virtual screening. J Chem Inf Model 46:243–253. https://doi.org/10.1021/ci0502855
52. Kuhn B, Kollman PA (2000) Binding of a diverse set of ligands to avidin and streptavidin: an accurate quantitative prediction of their relative affinities by a combination of molecular mechanics and continuum solvent models. J Med Chem 43:3786–3791. https://doi.org/10.1021/jm000241h
53. Sun H, Li Y, Tian S, Xu L, Hou T (2014) Assessing the performance of MM/PBSA and MM/GBSA methods. 4. Accuracies of MM/PBSA and MM/GBSA methodologies evaluated by various simulation protocols using PDBbind data set. Phys Chem Chem Phys 16:16719–16729. https://doi.org/10.1039/c4cp01388c
54. Sun H, Li Y, Shen M, Tian S, Xu L, Pan P, Guan Y, Hou T (2014) Assessing the performance of MM/PBSA and MM/GBSA methods. 5. Improved docking performance using high solute dielectric constant MM/GBSA and MM/PBSA rescoring. Phys Chem Chem Phys 16:22035–22045. https://doi.org/10.1039/c4cp03179b
55. Schrödinger. Command-line only scripts. https://www.schrodinger.com/scriptcenter. Accessed 4 Feb 2023
56. Shoichet BK (2004) Virtual screening of chemical libraries. Nature 432:862–865
57. Hosea NA, Jones HM (2013) Predicting pharmacokinetic profles using in silico derived parameters. Mol Pharm 10:1207–1215. https://doi.org/10.1021/mp300482w
58. Hosea NA, Jones HM (2013) Predicting pharmacokinetic profiles using in silico derived parameters. Mol Pharm 10:1207–1215. https://doi.org/10.1021/mp300482w
59. Lipinski CA, Lombardo F, Dominy BW, Feeney PJ (1997) Experimental and computational approaches to estimate solubility and permeability in drug discovery and development settings. Adv Drug Deliv Rev 23:3–25. https://doi.org/10.1016/s0169-409x(00)00129-0
60. Ertl P, Rohde B, Selzer P (2000) Fast calculation of molecular polar surface area as a sum of fragment-based contributions and its application to the prediction of drug transport properties. J Med Chem 43(20):3714–3717. https://doi.org/10.1021/jm000942e
61. Baell JB, Nissink JW (2018) Seven year itch: pan-assay interference compounds (PAINS) in 2017—utility and limitations. ACS Chem Biol 13(1):36–44. https://doi.org/10.1021/acschembio.7b00903
62. Hospital A, Goñi JR, Orozco M, Gelpí JL (2015) Molecular dynamics simulations: advances and applications. Adv Appl Bioinform Chem 8:37–47. https://doi.org/10.2147/AABC.S70333
63. Pearlman DA, Charifson PS (2001) Are free energy calculations useful in practice? A comparison with rapid scoring functions for the p38 MAP kinase protein system. J Med Chem 44:3417–3423. https://doi.org/10.1021/jm0100279
64. Taylor RD, Jewsbury PJ, Essex JW (2002) A review of protein-small molecule docking methods. J Comput Aided Mol Des 16:151–166. https://doi.org/10.1023/a:1020155510718
65. Wang E, Sun H, Wang J, Wang Z, Liu H, Zhang JZ, Hou T (2019) End-point binding free energy calculation with MM/PBSA and MM/GBSA: strategies and applications in drug design. Chem Rev 119(16):9478–9508. https://doi.org/10.1021/acs.chemrev.9b00055
66. Wang C, Greene DA, Xiao L, Qi R, Luo R (2018) Recent developments and applications of the MMPBSA method. Front Mol Biosci 4:87. https://doi.org/10.3389/fmolb.2017.00087

Terms and Conditions

Springer Nature journal content, brought to you courtesy of Springer Nature Customer Service Center GmbH (“Springer Nature”).
Springer Nature supports a reasonable amount of sharing of research papers by authors, subscribers and authorised users (“Users”), for small-scale personal, non-commercial use provided that all copyright, trade and service marks and other proprietary notices are maintained. By accessing, sharing, receiving or otherwise using the Springer Nature journal content you agree to these terms of use (“Terms”). For these purposes, Springer Nature considers academic use (by researchers and students) to be non-commercial.
These Terms are supplementary and will apply in addition to any applicable website terms and conditions, a relevant site licence or a personal subscription. These Terms will prevail over any conflict or ambiguity with regards to the relevant terms, a site licence or a personal subscription (to the extent of the conflict or ambiguity only). For Creative Commons-licensed articles, the terms of the Creative Commons license used will apply.
We collect and use personal data to provide access to the Springer Nature journal content. We may also use these personal data internally within ResearchGate and Springer Nature and as agreed share it, in an anonymised way, for purposes of tracking, analysis and reporting. We will not otherwise disclose your personal data outside the ResearchGate or the Springer Nature group of companies unless we have your permission as detailed in the Privacy Policy.
While Users may use the Springer Nature journal content for small scale, personal non-commercial use, it is important to note that Users may not:

1. use such content for the purpose of providing other users with access on a regular or large scale basis or as a means to circumvent access control;
2. use such content where to do so would be considered a criminal or statutory offence in any jurisdiction, or gives rise to civil liability, or is otherwise unlawful;
3. falsely or misleadingly imply or suggest endorsement, approval , sponsorship, or association unless explicitly agreed to by Springer Nature in writing;
4. use bots or other automated methods to access the content or redirect messages
5. override any security feature or exclusionary protocol; or
6. share the content in order to create substitute for Springer Nature products or services or a systematic database of Springer Nature journal content.

In line with the restriction against commercial use, Springer Nature does not permit the creation of a product or service that creates revenue, royalties, rent or income from our content or its inclusion as part of a paid for service or for other commercial gain. Springer Nature journal content cannot be used for inter-library loans and librarians may not upload Springer Nature journal content on a large scale into their, or any other, institutional repository.
These terms of use are reviewed regularly and may be amended at any time. Springer Nature is not obligated to publish any information or content on this website and may remove it or features or functionality at our sole discretion, at any time with or without notice. Springer Nature may revoke this licence to you at any time and remove access to any copies of the Springer Nature journal content which have been saved.
To the fullest extent permitted by law, Springer Nature makes no warranties, representations or guarantees to Users, either express or implied with respect to the Springer nature journal content and all parties disclaim and waive any implied warranties or warranties imposed by law, including merchantability or fitness for any particular purpose.
Please note that these rights do not automatically extend to content, data or other material published by Springer Nature that may be licensed from third parties.
If you would like to use or distribute our Springer Nature journal content to a wider audience or on a regular basis or in any other manner not expressly permitted by these Terms, please contact Springer Nature at

onlineservice@springernature.com